Chemical Geology 478 (2018) 131–147

Contents lists available at ScienceDirect

Chemical Geology

journal homepage: www.elsevier.com/locate/chemgeo

Origin of volatiles emitted by Plinian mafic eruptions of the Chikurachki volcano, Kurile arc, Russia: Trace element, boron and sulphur isotope constraints

Andrey A. Gurenko[a,b,*], Alexander B. Belousov[c], Vadim S. Kamenetsky[d,e], Michael E. Zelenski[e]

[a] Woods Hole Oceanographic Institution, Woods Hole, MA 02543, USA
[b] Centre de Recherches Pétrographiques et Géochimiques, UMR 7358, Université de Lorraine, 54501 Vandoeuvre-lès-Nancy, France
[c] Institute of Volcanology and Seismology, Petropavlovsk-Kamchatsky 683006, Russia
[d] School of Physical Sciences, University of Tasmania, Hobart, TAS 7001, Australia
[e] Institute of Experimental Mineralogy RAS, Chernogolovka 142432, Russia

ARTICLE INFO

Keywords:
Plinian mafic eruptions
Chikurachki volcano
Melt inclusions
Magmatic volatiles
Stable isotopes
Ion microprobe

ABSTRACT

Chikurachki is a 1816-m high stratovolcano on Paramushir Island, Kurile arc, Russia, which has repeatedly produced highly explosive eruptions of mafic composition. The present work is aimed at constraining the origin of volatile components (CO_2, H_2O, F, S, and Cl), along with B and S isotopic compositions in a series of phenocryst-hosted melt inclusions and groundmass glasses from basaltic andesite pyroclasts of the 1853, 1986, and prehistoric Plinian eruptions of the volcano. The ranges of volatile concentrations in melt inclusions (47–1580 μg/g CO_2, 0.4–4.2 wt% H_2O, 399–633 μg/g F, 619–3402 μg/g S and 805–1240 μg/g Cl) imply a sudden pressure release from ~460 through ~35 MPa that corresponds to ~1.2–16-km-depth range of magma ascent upon decompression. We conclude that rapid ascent of the volatile-rich basaltic magmas from ~16-km initial depth accompanied by near-surface bubble nucleation and growth, and subsequent magma fragmentation appear to be a primary reason for the Plinian character of the Chikurachki eruptions. Significant negative correlations of S with K, Zr, Nb, Ba, La, Ce, Pr ($R = -0.8$ to -0.9), no clear relationships of S with H_2O, CO_2 and Cl, but strong positive correlations of S/K_2O with H_2O/K_2O, Cl/K_2O and F/K_2O preclude magma degassing to be the only process affecting volatile concentrations dissolved in the melt. The $\delta^{34}S$ values of the studied inclusion and groundmass glasses range from −1.6 to +12.3‰, decrease with decreasing S, show significant positive correlations with H_2O/K_2O, Cl/K_2O and F/Zr, and negative correlations with a number of incompatible trace elements. Neither open- nor close-system magma degassing can account for the observed range of $\delta^{34}S$. The $\delta^{11}B$ values of the melt inclusions range from −7.0 to +2.4‰ with 13–23 μg/g B. The relationships of $\delta^{11}B$ with B/K_2O and B/Nb are inconsistent with magma contamination at shallow crustal depths. Linear character of 1/S vs. $\delta^{34}S$ relationship suggests two-component mixing. The possible mixing end-members could be the magmas having similar major and trace element compositions, but strongly contrasting volatile contents and S isotopes. Based on the behaviour of fluid-mobile vs. fluid-immobile incompatible trace elements, we conclude that the subduction component likely represents a mixture of subduction sediment-derived melt with up to 60% of slab-derived fluid. Admixture of ~1–8% of the inferred subduction component to the depleted mantle wedge source is required to account for the compositional range of the Chikurachki melt inclusions, and ~0.4–10% to constrain the composition of Kurile arc mafic magmas.

1. Introduction

Strongly explosive (Plinian) eruptions are characterised by high eruption rates, high eruption columns and widely dispersed fallout deposits, representing an efficient mechanism to transport volatiles from the Earth's interior to the upper atmosphere (Walker, 1973, 1980; Fisher and Schmincke, 1984; Wilson and Walker, 1987; Francis, 1993). Injection of water, halogens and sulphur into the atmosphere leads to the formation of solid and liquid aerosols, which may significantly affect global climate and the stability of the ozone layer (Brasseur and Granier, 1992). Plinian eruptions are mainly associated with water-rich intermediate and silicic magmas (andesite through dacite), whereas

* Corresponding author at: Centre de Recherches Pétrographiques et Géochimiques, 15, rue Notre-Dame des Pauvres, BP 20, 54501 Vandoeuvre-lès-Nancy, France.
E-mail address: agurenko@crpg.cnrs-nancy.fr (A.A. Gurenko).

http://dx.doi.org/10.1016/j.chemgeo.2017.10.009
Received 23 February 2017; Received in revised form 12 September 2017; Accepted 5 October 2017
Available online 07 October 2017

highly explosive eruptions of mafic composition (i.e., resembling basalt or basaltic andesite) are less common. Examples of Plinian mafic eruptions occur at Klyuchevskoy, Tolbachik, Chikurachki and Tyatya in the Kamchatka and Kurile arcs, Russia (Fedotov and Markhinin, 1983; Ovsyannikov and Muravyev, 1992; Belousov et al., 2003, 2015, 2017; Hasegawa et al., 2011), Masaya and Cerro Negro, Nicaragua (Williams, 1983; Roggensack et al., 1997), Arenal, Costa Rica (Soto and Alvarado, 2006; Szramek et al., 2006), Llaima, Chile (Ruth et al., 2016), Sumisu Rift, Japan (Gill et al., 1990), Ambrym, Vanuatu (Robin et al., 1993), Tofua, Tonga (Caulfield et al., 2011), Taupo and Tarawera, New Zealand (Walker, 1980; Walker et al., 1984), Shishaldin, Alaska (Szramek et al., 2010) and Etna, Italy (Houghton et al., 2004; Sable et al., 2006). The lack of clear relationships between eruption rate and style often associating with rapid change of eruptive behaviour of a volcano suggest that many different parameters such as conduit geometry, magma viscosity, changing conditions of magma ascent and fragmentation, and even the dynamics of *syn*-eruptive microlite growth may strongly affect the eruption figure (e.g., Fisher and Schmincke, 1984; Carey and Sparks, 1986; Houghton et al., 2004; Szramek et al., 2006, 2010; Houghton and Gonnermann, 2008).

The present work is a follow-up study to Gurenko et al. (2005a) and focuses on the detailed investigation of the behaviour of volatile components (CO_2, H_2O, F, S, and Cl) along with boron and sulphur isotopic compositions of the previously analysed olivine-, orthopyroxene- and plagioclase-hosted melt inclusions and groundmass glasses erupted by the Chikurachki volcano. Volatile-rich slab-derived melts and fluids play a central role in the origin of arc magmatism by lowering the solidus of a peridotite mantle wedge and triggering partial melting (e.g., Gill, 1981; McCulloch and Gamble, 1991; Hawkesworth et al., 1993; Pearce and Peate, 1995). Being a major inventory and a transport media of volatile components from descending plate to the overlying mantle, these melts and fluids (along with the factors listed above) may also have a link to the eruption style of volcanoes occurring in the subduction zone (SZ) setting. Here we explore the role of two concurrent processes, namely, subduction-related volatile flux versus possible gain of volatile components due to shallow crustal contamination of magma, also in relation of their possible contribution to the enrichment/depletion of the magma by sulphur and boron isotopes. Our new data provide additional constraints on the origin of volatile components in the mafic magmas erupted by the Chikurachki volcano during Plinian prehistoric and recent, 1853 and 1986 eruptions.

Another key problem in understanding the origin of arc magmas is the uncertainty in the provenance of volatile components. For example, Cl and H_2O are thought to be primarily (> 95%) from the subducting slab (e.g., Straub and Layne, 2003), whereas S and F can originate from metasomatically enriched subarc mantle or come directly from the slab (e.g., Alt et al., 1993; Métrich et al., 1999; Straub and Layne, 2003; Churikova et al., 2007; Selvaraja et al., 2017). Moreover, with increasing of subduction depth, the slab becomes progressively depleted in H_2O and Cl, and to a lesser extent in S and F, implying efficient fractionation of H_2O and Cl from S and F (e.g., Chaussidon et al., 1987; Métrich et al., 1999; Straub and Layne, 2003). Understanding the origin of volatiles that triggers the Plinian eruption of Chikurachki may also contribute to our understanding of fluid dynamics and mass transport in SZ settings, as well as help in elucidating the relative contributions of different subduction components to the generation of arc magmas.

2. Geological setting and samples

Chikurachki (50°19′24″N 155°27′39″E, 1816 m.a.s.l) is an active stratovolcano on Paramushir Island, the northern Kuriles (Fig. 1). The volcanism of Chikurachki results from westward subduction of the Pacific plate under the Okhotsk plate. The Late Holocene stratocone of the volcano is built on a thick sequence of Pleistocene lava flows (Gorshkov, 1967). The recorded activity on Chikurachki started around 7500 BCE. According to the Kamchatka Volcanic Eruption Response Team (KVERT), the most recent eruptions of 1958, 1961, 1964, 1973, 2002, 2003, 2004, 2005, 2007, 2008 were predominately of strombolian (mildly explosive), but recent Plinian (highly explosive) eruptions occurred in 1853, 1986 (Fig. 2), and the last one in 2015.

2.1. Samples studied

This study is based on the analyses of glassy lapilli with porphyritic texture, which came from the 1853 (sample CHK3/4), 1986 (sample CHK16) and two prehistoric (samples CHK13/1 and 13/2) tephra fallouts, resulting from documented, highly explosive eruptions of Chikurachki (Ovsyannikov and Muravyev, 1992; Belousov et al., 2003). We studied primary melt inclusions hosted by olivine, orthopyroxene and plagioclase phenocrysts, most of which were naturally quenched to glass. Chemical compositions of the studied inclusions and groundmass glasses (major and trace element, and H_2O, S and Cl concentrations) were reported by Gurenko et al. (2005a). Briefly, the erupted melts range from low- to medium-K tholeiitic basalts and andesites, which are typical for Kurile lavas (Fig. S2.1 – Supporting online material). Variation diagrams of FeO, CaO and K_2O vs. SiO_2 show that glass compositions follow simple trends of magma fractionation (Fig. 5 in Gurenko et al., 2005a). The phenocrysts are dominated by euhedral, elongated, twinned individual crystals of plagioclase (Pl, ~0.2–3.0 mm, 70–90 vol %, $An_{74–95}$) that may also form glomerocrysts. Phenocrysts of subhedral to rounded olivine (Ol, $Fo_{72–78}$) and orthopyroxene (Opx, *mg*-number = 72–75), both of 0.2–0.5 mm size, and euhedral to resorbed clinopyroxene (Cpx, 0.3–1.0 mm, *mg*-number = 71–77) are present in subordinate amounts. The groundmass is strongly vesiculated (20–30 vol% vesicles) and consists of variable proportions of rounded olivine, prismatic augite and isometric Fe-Ti oxide crystals mixed with needle-like plagioclase microlites (up to 200 μm).

The studied inclusion and groundmass glasses are slightly enriched in light rare earth elements (LREE) relative to heavy rare earth elements (HREE); e.g., $[La/Sm]_n$ = 1.8–2.4, where the subscript *n* denotes the respective element concentrations normalised to those of N-MORB taken from Hofmann, 1988 (Fig. 3, Table S2.1 – Supporting online material). The glasses also show significant depletions in high-field-strength elements (HFSE) relative to LREE, but nearly equal concentrations of HFSE relative to HREE normalised to N-MORB (e.g., $[Nb/La]_n$ = 0.19–0.29, $[Zr/Sm]_n$ = 0.52–0.76, $[Y/Yb]_n$ = 0.86–1.24), and enrichments in Th and large-ion lithophile elements (LILE) relative to Nb (e.g., $[Ba/Nb]_n$ = 41–69, $[Th/Nb]_n$ = 7–30, $[K/Nb]_n$ = 15–25 and $[Sr/Sm]_n$ = 2.9–6.9). The inclusions, and to lesser extent the groundmass glasses are characterised by relatively high contents of volatile components (the concentrations of B, H_2O, Cl and F shown in Fig. 3 are discussed in Section 4.1), displaying positive anomalies in the multi-element diagram relative to respective trace elements of similar incompatibility (e.g., $[Cl/Nb]_n$ = 21–54, $[B/K]_n$ = 2.3–5.4, $[H_2O/Ce]_n$ = 4.9–23, $[F/Nd]_n$ = 2.2–3.2, $[F/Zr]_n$ = 3.9–7.8). These values are generally in, or slightly exceeding, the range of volatile concentrations reported for the Kurile island arc basalts and basaltic andesites (MgO > 2.5 wt%) by Bailey et al. (1987a, 1987b), Ishikawa and Tera (1997), Ikeda (1998), Ikeda et al. (2000), Takagi et al. (1999), Ishikawa et al. (2001) (Fig. 3).

3. Analytical methods

Ion microprobe analyses were obtained with a CAMECA IMS 1280 ion microprobe at the Northeast National Ion Microprobe Facility (Woods Hole Oceanographic Institution, Woods Hole, USA) (for detailed description of the employed analytical protocols, see Supporting online material).

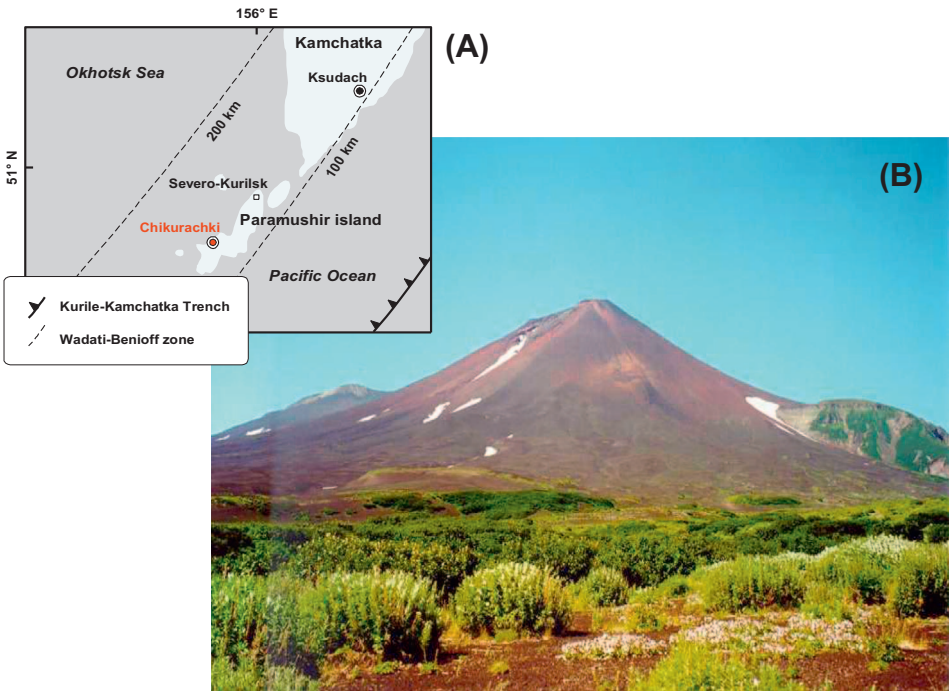

Fig. 1. (A) Schematic map of the northern Kurile Islands (Russia) with the locality of the Chikurachki volcano on Paramushir Island shown in relation to the Kamchatka Peninsula. Contours show isobars for the top of the Wadati-Benioff zone from Tatsumi et al. (1994). (B) The Chikurachki volcano, a view from the eastern side ~6 km away.

4. Results

4.1. Volatile concentrations

The concentrations of CO_2, H_2O, F, S, and Cl in naturally quenched, glassy inclusions hosted in Ol, Opx and Pl are listed in Table S2.1 (Supporting online material), along with H_2O, S and Cl reported by Gurenko et al. (2005a). The inclusions have a wide range of volatile concentrations (39–653 μg/g CO_2, 0.4–4.2 wt% H_2O, 428–638 μg/g F, 676–3450 μg/g S, and 805–1243 μg/g Cl) that corresponds to the volatile contents previously reported by Gurenko et al. (2005a). Correction for post-entrapment crystallisation (PEC) of host mineral (up to 7.8 wt% Ol, 0.8 wt% Opx, and no correction for Pl) results in the following ranges: 39–626 μg/g CO_2, 0.4–4.2 wt% H_2O, 412–634 μg/g F, 639–3408 μg/g S, 805–1241 μg/g Cl, which appeared to be nearly the same (given the maintained analytical uncertainty) as the uncorrected volatile concentrations. This observation implies that the eruption and quenching of magma occurred shortly after the inclusions have been entrapped by growing phenocrysts. Thus, the concentrations of H_2O and CO_2 measured in the studied melt inclusions reflect the last vapour-melt equilibrium in the magmatic system upon the eruption, returning a minimum pressure of magma fractionation. According to the *VolatileCalc* solution model (Newman and Lowenstern, 2002), they correspond to H_2O-CO_2 gas pressure of 33 to 276 MPa or to the range of depth from ~1 to ~9.5 km, assuming average and constant density of ~2900 kg/m^3 of the upper crust (Fig. 4A).

Several recent studies (Esposito et al., 2011; Steele-Macinnis et al., 2011; Hartley et al., 2014; Moore et al., 2015; Wallace et al., 2015; Mironov et al., 2015; Aster et al., 2016) have demonstrated that 40 to 90% of the original CO_2 dissolved in the melt at the time of inclusion entrapment can be lost to a shrinkage bubble during post-entrapment cooling. A correction algorithm described by Wallace et al. (2015) was therefore used to reconstruct the original CO_2 and H_2O concentrations in the entrapped melts (see Supporting online material). These calculations revealed that ~5 to 69% of the original CO_2 and 0.1 to 3.2% of the original H_2O could have been lost to the shrinkage bubble, in agreement with the results of the above studies. The following ranges of volatile concentrations were obtained after the correction: 47–1580 μg/g CO_2, 0.4–4.2 wt% H_2O, 399–633 μg/g F, 619–3402 μg/g S and 805–1240 μg/g Cl (Table S2.1 – Supporting online material). According to the *VolatileCalc* solution model (Newman and Lowenstern, 2002), the corrected results correspond to the H_2O-CO_2 gas pressures between 35 and 456 MPa or to ~1.2–15.7-km-range of crustal depth (Fig. 4B).

The concentrations of S in melt inclusions are shown in comparison with mid-ocean ridge basalts (MORB) and ocean island basalts (OIB) (Fig. 5A). Many of the Chirurachki glass inclusions have similar or higher S concentrations than those of MORB or OIB, whereas all groundmass glasses are depleted in S (< 350 μg/g), consistent with sulphur loss presumably by degassing. However, sulphur in the inclusion glasses shows significant negative correlations with a number of trace and rare earth incompatible elements, such as K (−0.81), Ti (−0.59), Y (−0.61), Zr (−0.82), Nb(−0.71), Ba (−0.83), La (−0.79), Ce (−0.88), Pr (−0.77), Nd (−0.71), Sm (−0.68), Gd (−0.56), Dy (−0.73), Ho (−0.53), Er (−0.73), Yb (−0.66), Lu (−0.71), Th (−0.66), where the respective correlation coefficient (R) values are given in brackets and N = 21, if not specified (Fig. 5B and Table S2.1 – Supporting online material). All these correlations are significant at 95% confidence level (for N = 18 and 21, a number of points in the correlations, a critical value of the Pearson correlation coefficient at the 0.05-level of significance for a two-tailed test is 0.47 and 0.43, respectively). There are no significant correlations of S with H_2O, Cl and F. We observe, however, strong positive correlation between these elements, if their concentrations are normalised to K_2O (or any other melt- and fluid-immobile incompatible element) that minimises possible effects of partial melting and/or magma fractionation (e.g., R = 0.83 for S/K_2O vs. H_2O/K_2O correlation, Fig. 5C, R = 0.80 for S/K_2O vs. Cl/K_2O, Fig. S2.2A – Supporting online material, R = 0.85 for S/K_2O vs. F/K_2O, Fig. 5D, and R = 0.88 for Cl/K_2O vs. H_2O/K_2O, Fig. 5E). Chlorine does not correlate with incompatible trace elements, except for Sr (R = −0.56; Fig. S2.2B – Supporting online material), shows a significant correlation with fluorine (R = 0.70; Fig. S2.2C – Supporting online material), which becomes much stronger, if we consider F/Zr vs. Cl/Nb ratios (R = 0.88; Fig. 5F).

4.2. Sulphur isotopes

Sulphur isotopic compositions of the studied melt inclusions and one groundmass glass are given in Table S2.1 (Supporting online

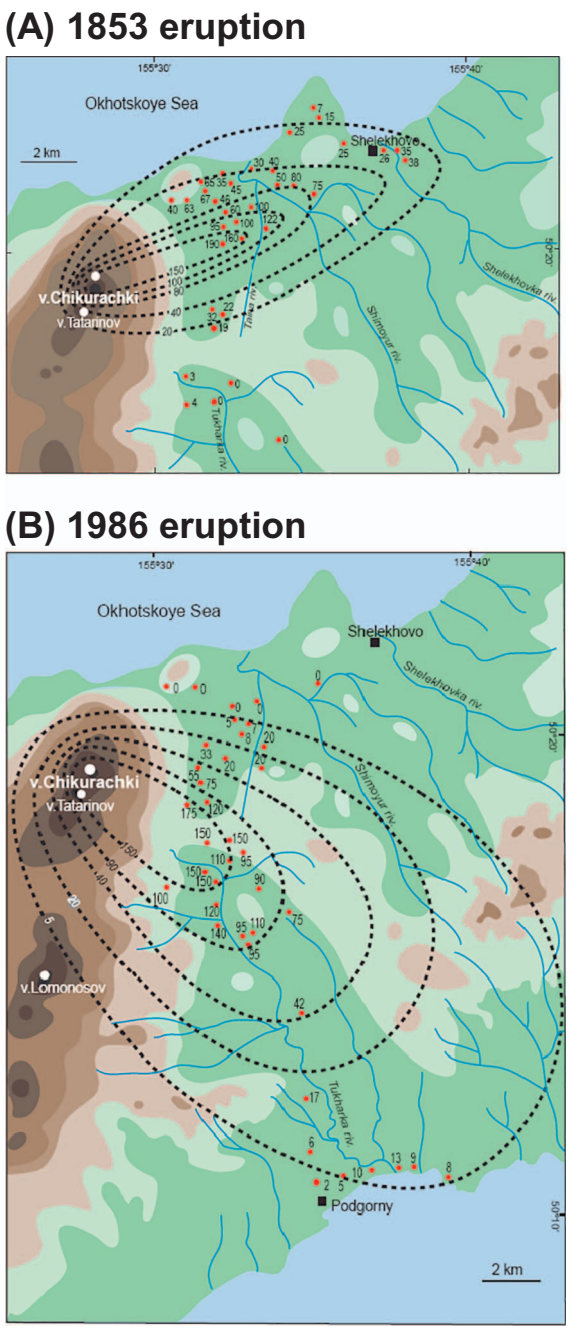

Fig. 2. Isopachs (lines of equal thickness) given in cm of the tephra representing Plinian (A) 1853 and (B) 1986 eruptions of the Chikurachki volcano after Belousov et al. (2003).

material) and presented in Fig. 6. The $\delta^{34}S$ values are given in permil units (‰) relative V-CDT (the Vienna Canyon Diabolo Troilite, $^{34}S/^{32}S = 0.0441626 \pm 0.0000039$; Ding et al., 2001). The $\delta^{34}S$ values of the inclusion glasses range from −1.6 to +12.3‰, and decrease with decreasing S concentrations ($R = 0.85$; Fig. 6A). The S vs. $\delta^{34}S$ relationship has a hyperbolic shape and is transformable into a straight line in the 1/S-$\delta^{34}S$ space (Fig. 6B), pointing towards two-component mixing scenario (Langmuir et al., 1978), though the effect of magma degassing cannot be completely excluded (see further discussion). The sample 13/1 matrix glass has $\delta^{34}S = +0.39 \pm 0.43$‰, 1 SE, contains very low S concentration (107 μg/g S) and strongly deviates from the linear array defined by melt inclusions (Fig. 6B), being in contrast strongly degassed. Also, the $\delta^{34}S$ values show significant positive correlations with H_2O (0.54), CO_2 (0.55) and Sr (0.5), as well as negative correlations with light lithophile elements Li (−0.53, $N = 10$), Be (−0.73, N = 10) and B (−0.6), and other incompatible elements, such as K (−0.8), Zr (−0.71), Nb (−0.64), Ba (−0.75), La (−0.69), Ce (−0.72), Pr (−0.57), Sm (−0.63), Gd (−0.76), Dy (−0.71), Tb (−0.49), Er (−0.8), Lu (−0.79), Th (−0.53), where the respective correlation coefficient (R) values are given in brackets and $N = 17$, if not specified, and the critical value of the Pearson correlation coefficient is 0.48. The significance of the correlations of $\delta^{34}S$ with volatile components becomes higher, if volatile concentrations are normalised to incompatible elements as, for instance, H_2O/K_2O (0.79), Cl/K_2O (0.83) (Fig. 6B,C), F/Zr (0.84, Fig. S2.2D – Supporting online material).

4.3. Boron concentrations and B isotopic composition

The concentrations of boron (12.5–22.9 μg/g measured, and 12.5–21.7 μg/g corrected for PEC) are similar to those previously reported by Gurenko et al. (2005a) (16.1–18.7 μg/g B) (Table S2.1 – Supporting online material). The B/K ratios ranging from 0.0025 to 0.0057 are systematically higher than those of primitive N-MORB (B/K of ~0.001) and OIB (B/K of ~0.0003) (Ryan and Langmuir, 1993; Chaussidon and Jambon, 1994; Gurenko and Chaussidon, 1997), but are in the midrange of B concentrations reported for Kurile arc magmas with SiO_2 < 60 wt% (4.5–36.6 μg/g B; Ryan et al., 1995; Ishikawa and Tera, 1997). Very similar concentrations of B in the Chikurachki lavas (14.4–15.5 μg/g) were found, in particular, by Ishikawa and Tera (1997), who also noted a clear across-arc variation of B/Nb ratios (and $\delta^{11}B$, as well). At the slab depth of ~140 km corresponding to that of the Chikurachki volcano (e.g., Tatsumi et al., 1994; Ishikawa and Tera, 1997; Ishikawa et al., 2001 and references therein), the B/Nb ratios in the Kurile lavas vary from ~6 to 18 (Ishikawa and Tera, 1997), and the present B/Nb range obtained for the studied melt inclusions (from ~9 to ~22) is in agreement with these data.

The $\delta^{11}B$ values of the studied naturally quenched olivine-hosted melt inclusions range from −7.0 to +2.4‰, calculated relative to NBS 951 standard with $^{11}B/^{10}B = 4.04558 \pm 0.00033$ (Spivack and Edmond, 1986) (Table S2.1 – Supporting online material). The range is similar, but extends to more negative values than those of the Kurile arc lavas (from −3.8 to +5.9‰; Ishikawa and Tera, 1997), being however within a broad interval of $\delta^{11}B$-values of arc magmas worldwide, from −21.3‰ (e.g., Mt. Shasta; Rose et al., 2001) to +12‰ (e.g., Izu arc; Straub and Layne, 2002). In contrast to S isotopes, $\delta^{11}B$ values show neither a correlation with the concentrations of B or 1/B values nor with major and incompatible trace elements. Similarly, a wide $\delta^{11}B$ range of ~20‰ (from −21.3 to −1.1‰ at relatively narrow range of boron concentrations (0.67–1.64 μg/g B) showing no clear correlation between each other was described in the Mt. Shasta basaltic andesite rocks (Rose et al., 2001).

5. Discussion

5.1. H_2O-Cl-B and $\delta^{11}B$ relationships and the magma contamination scenario

Assimilation of crustal rocks is a common process that can significantly modify pristine chemical and isotopic compositions of parental arc magmas (e.g., Davidson, 1987; Thirlwall et al., 1996; Hickey et al., 1986; Turner et al., 1997; Macpherson and Mattey, 1998; Vroon et al., 2001; Bindeman et al., 2004; Walowski et al., 2016). Excess of halogens in mafic magmas, and especially coherent variation of H_2O and Cl was shown to be a good proxy to assess the role of assimilation of oceanic crust and/or addition of NaCl-rich brines or fluids during magma fractionation (e.g., Anderson, 1974; Michael and Schilling, 1989; Jambon et al., 1995; Michael and Cornell, 1998; Kent et al., 1999; Lassiter et al., 2002; Simons et al., 2002; le Roux et al., 2006; Shimizu et al., 2009; Gurenko and Kamenetsky, 2011; Kendrick et al., 2013; Cabral et al., 2014).

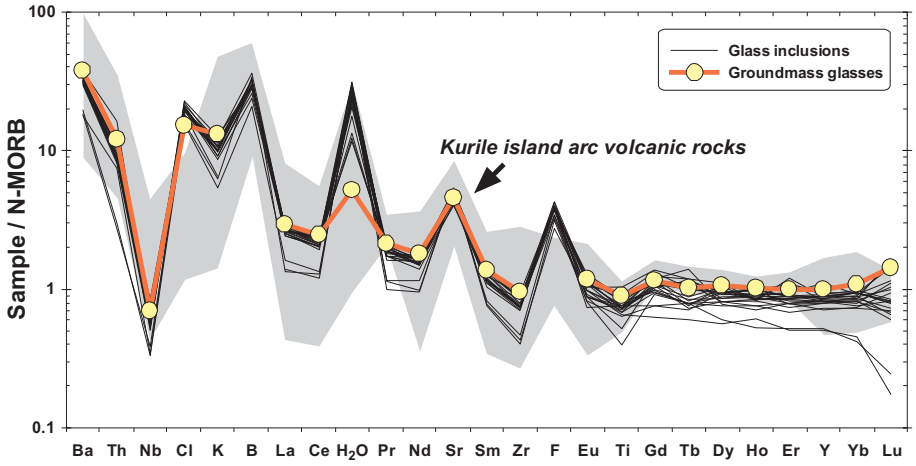

Fig. 3. Multi-element diagram presenting trace and rare-earth element distribution in olivine-hosted glass inclusions and groundmass glasses and demonstrating positive H_2O, B, Cl and F enrichment. The concentrations of trace elements in N-MORB used for normalisation are from Hofmann (1988), the normalisation values for volatile elements and water are 1350 μg/g H_2O, 0.6 μg/g B, 54.5 μg/g Cl, and 146 μg/g F, which were calculated from the average B/K ≈ 0.001, H_2O/Ce ≈ 180, K/Cl ≈ 11, and F/Nd ≈ 20, or F/Zr ≈ 2 ratios inferred for MORB using the data of Ryan and Langmuir, 1993, Jambon et al., 1995, Saal et al., 2002, Kendrick et al., 2013, Le Voyer et al., 2015 and references therein. The shaded field presents whole-rock data for the Kurile island arc basalts and andesites (MgO > 2.5 wt%) from Bailey et al. (1987a, 1987b), Ishikawa and Tera (1997), Ikeda (1998), Ikeda et al. (2000), Takagi et al. (1999), Ishikawa et al. (2001).

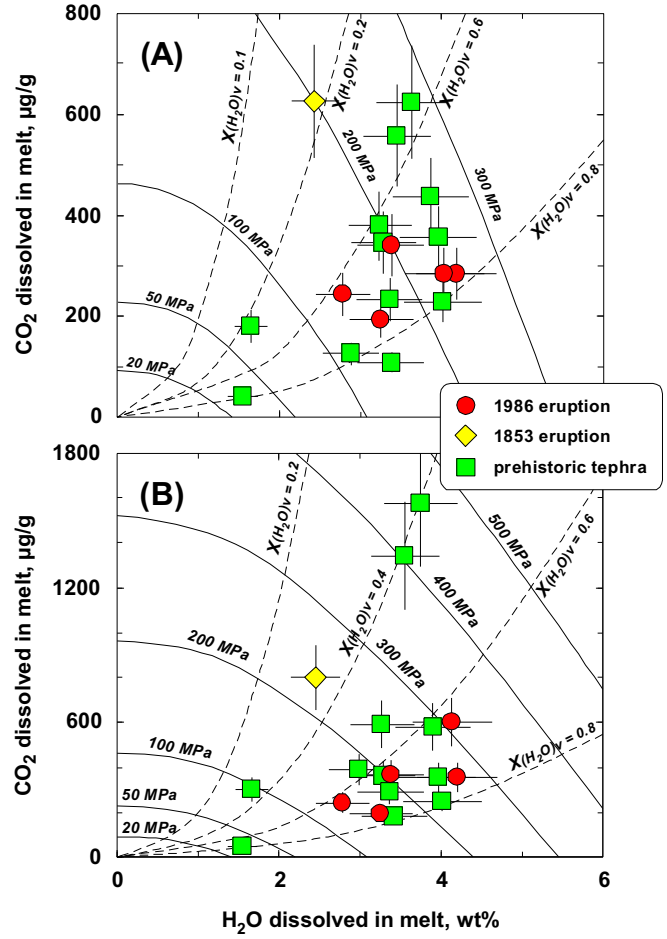

Fig. 4. Concentrations of CO_2 and H_2O dissolved in glass inclusions measured by SIMS. (A) CO_2 and H_2O corrected for the amount of host mineral crystallised inside melt inclusions between entrapment and magma eruption and final quenching. (B) CO_2 and H_2O corrected for the loss of volatiles to the inclusion shrinkage bubble (see text). Isobars of melt compositions in equilibrium with CO_2-H_2O fluid (*solid lines*) and isopleths of fluid composition (dashed lines with labels returning molecular fraction of H_2O in the fluid) were calculated using *VolatileCalc* solution model (Newman and Lowenstern, 2002). The isopleths and isobars were calculated for basaltic magma composition at 1000°C i.e., the average temperature of the Chikurachki magmas (Gurenko et al., 2005a). *Error bars* represent ± 2*σ* average integral analytical uncertainty, i.e., ± 18% relative for CO_2 and ± 12% relative for H_2O, they are less than the size of a symbol, if not shown.

A positive correlation of H_2O/K_2O with Cl/K_2O in the Chikurachki melt inclusions (Fig. 5E) can be also interpreted in favour of magma contamination. The results of modelling of magma contamination using different compositions of probable crustal contaminants are shown in Figs. 7 and 8. In the modelling, we use the same element concentrations and $\delta^{11}B$ values of seawater (*SW*), 15%- and 50%-NaCl brine (labeled in the figures as *15%-NaCl* and *50%-NaCl*, respectively), and altered oceanic crust (*AOC*) mixing end-members, as in Gurenko and Kamenetsky (2011) (Table 1). Given the narrow range of incompatible element concentrations in the studied melt inclusions (Fig. 3), the concentrations of K_2O (0.804 wt%), Nb (1.28 μg/g) and Ce (15.37 μg/g) of a presumably "uncontaminated" arc magma (*UAM*) were defined as average of all melt inclusions from Table S2.1 – Supporting online material (using PEC-corrected concentrations). The boron content and B isotopic composition of *UAM* (0.9 μg/g B, $\delta^{11}B = -3.7‰$) corresponding to back-arc basin basalts presumably unaffected by later shallow-crustal contamination were taken from Chaussidon and Marty (1995). The concentrations of H_2O and Cl in *UAM* were calculated using those of the neighbouring elements of similar incompatibility, but showing no anomalies in the multi-element diagram (Fig. 3), to be in the lower left corner of the respective panels in Fig. 7 and matching the lower end of the trends defined by the inclusion compositions: $[H_2O]_n = ([Ce]_n \times [Pr]_n)^{0.5}$, equal to 0.256 wt% H_2O, and $[Cl]_n = ([Nb]_n \times [K]_n)^{0.5}$, equal to 128.5 μg/g Cl. The chemical and isotopic compositions of seawater is relatively uniform and well constrained, whereas the composition of seawater-derived NaCl-brines can be calculated from that of *SW* (Table 1). In contrast, the composition of altered oceanic crust is variable. In particular, *AOC* from Gurenko and Kamenetsky (2011) is significantly more H_2O-, Cl- and K_2O-rich than that used for similar calculations by le Roux et al. (2006). In order to account for possibly wider ranges of H_2O, Cl, Nb and Ce, we considered two compositions of *AOC*: *AOC1* from Gurenko and Kamenetsky (2011) and *AOC2* from le Roux et al. (2006) (Table 1). Finally, we assigned a composition of siliceous marine sediment (*SED*), which is considered as one possible, if not a single contamination component to account for the negative $\delta^{11}B$ melt inclusion values, with 10.1 wt% H_2O, 1.7 wt% K_2O, 7.67 μg/g Nb, 50.11 μg/g Ce. The concentrations of H_2O, K_2O, Nb and Ca used in calculations are those of the average sediment column of the Kurile trench from Plank and Langmuir, 1998, and 1000 μg/g Cl, 120 μg/g B, and $\delta^{11}B = -10‰$ were taken from Gurenko and Kamenetsky, 2011, given that siliceous terrigenous sediments may be as low as −15‰ of $\delta^{11}B$ (Leeman and Sisson, 1996).

As noted by Gurenko and Kamenetsky (2011), it is not possible to unequivocally prove magma contamination only on the basis of H_2O/K_2O vs. Cl/K_2O relationships (or using Cl- and H_2O-to-incompatible-element normalised ratios). If we consider solely the H_2O/K_2O-Cl/K_2O variations in melt inclusions (Fig. 7A) or equally, H_2O/Ce-Cl/Nb

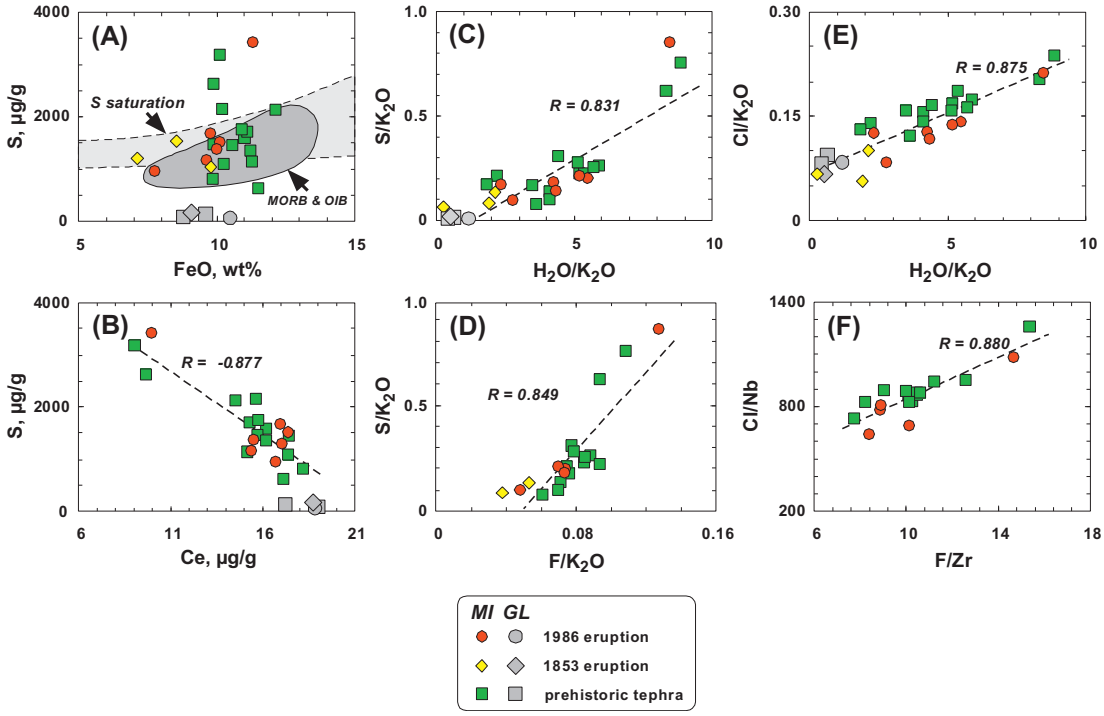

Fig. 5. Concentrations of S, Cl and F in glass inclusions and lapilli matrix glasses. (A) FeO vs. S variations. The larger shaded grey symbols denote the compositions of the respective host matrix glasses. The *MORB and OIB* shaded field presents data for presumably undegassed MORB and Hawaiian submarine tholeiitic and alkali basaltic glasses from Wallace and Carmichael (1992). The *S saturation* shaded field represents compositional dependence of sulphur saturation of MORB-type magmas with immiscible sulphide liquid of pure FeS based on experimental data of Smythe et al. (2017) and references therein. Legend: *MI* = melt inclusions, *GL* = matrix glasses. (B) Ce vs. S, (C) H_2O/K_2O vs. S/K_2O, (D) F/K_2O vs. S/K_2O, (E) H_2O/K_2O vs. Cl/K_2O, and (F) F/Zr vs. Cl/Nb. The observed relationships do not support shallow-depth contamination of the magma, and rather favour a deep origin of volatiles resulted from slab-derived fluid released during subduction (see text).

variations (Fig. 7B), they can be explained by contamination of magma by seawater or NaCl-rich brines. On the other hand, if in addition to H_2O and Cl we consider boron content and B-isotope data i.e., H_2O/K_2O vs. B/K_2O variations (Fig. 7C) (or equally, H_2O/Ce-B/Nb variations; Fig. 7D) together with B/K_2O (or B/Nb) vs. $\delta^{11}B$ data (Fig. 8), then the relationships with boron confirm neither the contribution of seawater and seawater-derived components, nor the contribution of *AOC1*, *AOC2* and *SED*. Indeed, to account for the compositions of melt inclusions with strongly and coherently varying H_2O/K_2O = 0.3–8.9 and Cl/K_2O = 0.06–0.24, it would require contamination either by *SW* (up to 7%) or more concentrated NaCl-brine, or assimilation of *AOC1* (up to 60%) or both *AOC1* + *SW* components (Fig. 7A). No significant effect of *15%-NaCl* and *50%-NaCl* brine, as well as the role of *AOC2* and *SED* can be recognised in this diagram. The same conclusions can be derived from the H_2O/Ce vs. Cl/Nb variations (Fig. 7B), with only a difference that contamination by *AOC1* (up to 70%) is required. However, if we consider mixing of the same components in coordinates H_2O/K_2O vs. B/K_2O or H_2O/Ce vs. B/Nb (Fig. 7C,D), then the role of *SW* and *AOC1*, along with *15%-NaCl* and *AOC2* is not yet justified, but the *50%-NaCl* end-member appears to be potentially significant. The amount of *SED* to add to *UAM* appears to be up to 50% in Fig. 7C and up to 100% in Fig. 7D, both being unrealistic. Finally, if we consider B/K_2O vs. $\delta^{11}B$ or B/Nb vs. $\delta^{11}B$ systematics (Fig. 8), then the role of seawater, NaCl-brines and *AOC1* is not confirmed at all, while the amount of *AOC2* and *SED* to be assimilated approaches to 100% (Fig. 8B).

In conclusion, we note that Cl and F often behave as incompatible elements during partial melting and magma fractionation (e.g., Fisher and Schmincke, 1984; Carroll and Webster, 1994; Jambon, 1994; Dalou et al., 2014). As shown by Dalou et al. (2014 and references therein), a Cl/F ratio of > 1 is expected in arc magmas resulting from partial melting of a depleted mantle source mixed with an aqueous dehydration fluid because the Cl/F ratio in the subduction slab fluids is usually high (e.g., ~4 in Mount Shasta rocks and up to 9.5 in Izu Bonin arc magmas). In contrast, the low Cl/F ratios (< 1; e.g., Central and South American arcs, Kermadec) suggest that the magmas were produced by melting of a mantle source mixed with a hydrous slab melt. In this context, it is essential to note that Cl/F ratios in the studied melt inclusions range from 1.5 to 2.0, pointing towards predominant role of the subduction slab fluid in the origin of Chikurachki magmas. Finally, the observed relationships of S/K_2O with K_2O-normalised concentrations of H_2O, Cl and F (Fig. 5C,D and Fig. 2.2A – Supporting online material), as well as the H_2O/K_2O vs. Cl/K_2O and F/Zr vs. Cl/Nb correlations (Fig. 5E,F) strongly suggest that the variations of H_2O, S, Cl and F contents were not primarily affected by degassing or contamination, but more likely related to the transport of these components to magma source region by subduction slab fluids, in agreement with the previous studies of the Kurile-Kamchatka arc volcanism (e.g., Hochstaedter et al., 1996; Ishikawa and Tera, 1997; Kepezhinskas et al., 1997; Dorendorf et al., 2000; Churikova et al., 2001, 2007; Ishikawa et al., 2001; Portnyagin et al., 2007, 2015; Konrad-Schmolke et al., 2016).

5.2. Origin of sulphur concentration and S-isotope ranges

Sulphur solubility in basaltic magmas was shown to be mostly a function of iron content of the melt, if sulphur is predominately present in sulphide (S^{2-}) form (e.g., Connolly and Haughton, 1972; Haughton et al., 1974; Mathez, 1976; Carroll and Rutherford, 1985; Wallace and Carmichael, 1992), but it also depends strongly on temperature, pressure, redox conditions, H_2O content, and the composition of coexisting melt and vapour phase (Nagashima and Katsura, 1973; Katsura and Nagashima, 1974; Carroll and Rutherford, 1985, 1987; Luhr, 1990; Wallace and Carmichael, 1992; Mavrogenes and O'Neill, 1999; Matjuschkin et al., 2016; Canil and Fellows, 2017; Mavrogenes and Blundy, 2017). The solubility of sulphur is generally higher (at a given oxygen fugacity, fO_2) in mafic (tholeiite and hawaiite), as compared to

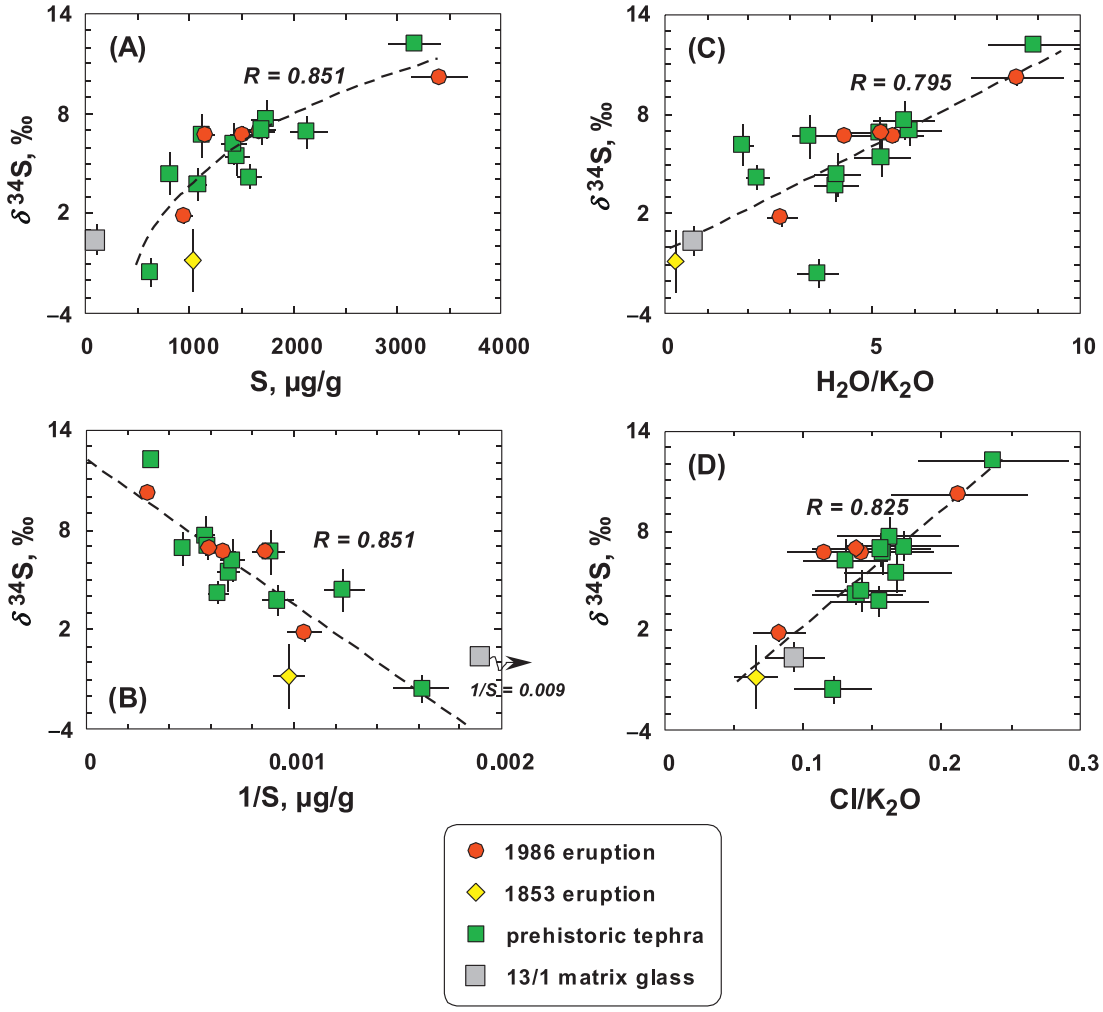

Fig. 6. Sulphur isotope composition of glass inclusion and one host matrix glass of the Chikurachki prehistoric eruption related to (A) S concentrations, (B) H_2O/K_2O and (C) Cl/K_2O ratios.

more SiO_2-rich magmas (rhyodacite) (e.g., Katsura and Nagashima, 1974).

As a sulphide-saturated melt becomes progressively oxidised, higher amount of sulphur is required to be dissolved in the melt to cause saturation of the melt with sulphide (e.g., Carroll and Webster, 1994 and references therein). This is also evident from the exponential character of FeO-S relationships observed in the more S-rich inclusions (Fig. 5A). The sulphur valence state changes from S^{2-} to S^{6+} within a limited range of oxygen fugacity, from NNO − 1 to NNO + 2 (Carroll and Rutherford, 1988; Wallace and Carmichael, 1994; Metrich and Clocchiatti, 1996; Gurenko and Schmincke, 2000; Jugo et al., 2005a, 2005b, 2010; Fiege et al., 2015). Further melt oxidation causes a sulphide phase to become unstable. At these and more oxidised conditions (i.e., fO_2 is greater than NNO + 2), anhydrite ($CaSO_4$) may become stable and appear as phenocrysts in the magma, as it was observed, for example, in some El Chichón and Mount Pinatubo trachyandesite and dacite magmas (Luhr et al., 1984; Varekamp et al., 1984; Carroll and Rutherford, 1987; Luhr, 1990; Bernard et al., 1991; Kress, 1997). Moreover, the solubility of sulphate (SO_4^{2-}) is much higher than that of sulphide (S^{2-}) in mafic magmas and can reach up to 2.5 wt% SO_3 (Carroll and Rutherford, 1985, 1987; Luhr, 1990; Metrich and Clocchiatti, 1996; Gurenko and Schmincke, 2000; Jugo et al., 2005a, 2005b; Fiege et al., 2015). Since S concentrations in many of our inclusion glasses significantly exceed the level of S^{2-} solubility, and they show no correlation with FeO (Fig. 5A), we contend that a significant proportion of sulphur is dissolved as SO_4^{2-} species. This is consistent with generally higher oxidation state of subduction-zone-related magmas, and also with previously estimated oxygen redox conditions of the Chikurachki magmas (i.e., ΔNNO = +1 to +2; Gurenko et al., 2005a). According to the relationship given in Wallace and Carmichael (1994):

$$\log (X_{SO_4^{2-}}/X_{S^{2-}}) = a \ \log \ fO_2 + b/T + c \quad (1)$$

where $X_{SO_4^{2-}}$ and $X_{S^{2-}}$ are mole fractions of SO_4^{2-} and S^{2-} sulphur species in the melt (i.e., $X_{SO_4^{2-}} + X_{S^{2-}} = 1$), T is temperature in Kelvin, and coefficients $a = 1.02$, $b = 25{,}410$, and $c = -10$, between 80 and 98% sulphur dissolved as SO_4^{2-} is expected in the basaltic melts representing the studied Plinian 1986, 1853 and prehistoric eruptions of the Chikurachki volcano, thereby explaining the elevated concentrations of sulphur in the studied melt inclusions.

The fact that sulphur isotopic composition (i.e., $\delta^{34}S$) strongly correlates with S concentrations in the melt inclusions and groundmass glasses (Fig. 6A,B), as well as with K_2O-normalised concentrations of H_2O and Cl (Fig. 6C,D) suggests that sulphur was more likely introduced to the magma by the same process along with H_2O and Cl. One possible and relatively simple explanation would be a contamination of magma by sulphate-bearing seawater-derived material at shallow-crustal depth, as it was previously demonstrated on example of Miocene basaltic hyaloclastites drilled during the ODP Leg 157 southwest of Gran Canaria (Canary Islands, Spain) by Gurenko et al., 2001. However, as discussed above, shallow-depth contamination was not a factor controlling budget of volatile components in the studied Chikurachki

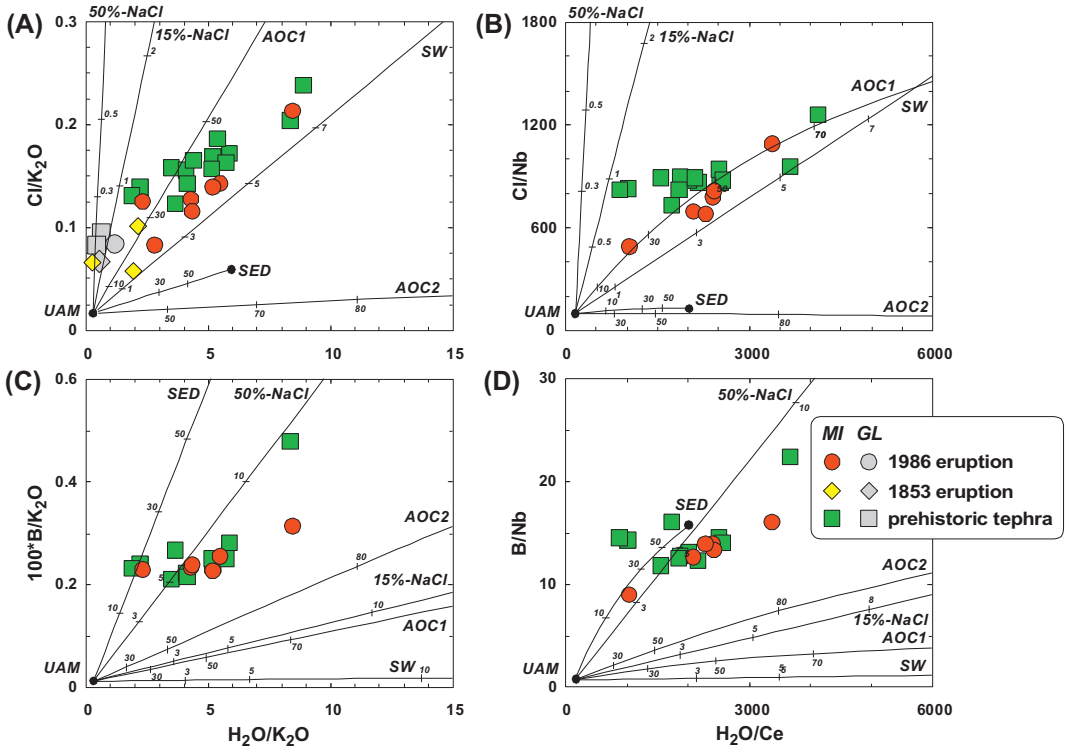

Fig. 7. Diagrams of (A) H_2O/K_2O vs. Cl/K_2O, (B) H_2O/Ce vs. Cl/Nb, (C) H_2O/K_2O vs. B/K2O, and (D) H_2O/Ce vs. B/Nb (given as weight ratios) illustrate the effects of contamination (mixing lines) of presumably "uncontaminated" arc magma (*UAM*) with different types of contaminants, i.e., seawater (*SW*), 15%- and 50%-NaCl saline brines (labelled as *15%-NaCl* and *50%-NaCl*, respectively), altered oceanic crust (*AOC1* and *AOC2*) and siliceous marine sediment (*SED*) (see text and Table 1 for the end-member chemical compositions and further details). Numbers on the mixing lines refer to wt% of the contaminant added to the magma. The calculated mixing trends allow us to conclude that direct contamination of UAM by altered basaltic rocks and marine sediments at shallow depth and/or by seawater or seawater-derived components (saline brine) is unable to account for the H_2O, Cl and B enrichment observed in the studied melt inclusions. Legend: *MI* = melt inclusions, *GL* = matrix glasses.

magmas. Thus, the origin of sulphur and its S-isotope signature could more likely be ascribed to slab-derived fluids. Whether a consequent degassing of the magmas could result in the observed, nearly 14‰-range of $\delta^{34}S$ values is a subject of further discussion.

5.2.1. S-isotope fractionation during magma degassing

Magma degassing is an alternative process, which is capable to significantly affect the concentration and isotopic composition of sulphur in the melt by changing the proportion of the reduced (S^{2-}) and oxidised (SO_4^{2-}) forms (e.g., Taylor, 1986; Marini et al., 2011; Mandeville et al., 2009 and references therein). This is mostly because sulphide and sulphate species may possess strongly contrasting $\delta^{34}S$ values, with an average fractionation factor of + 7.3 ± 1.4‰ between sulphate and sulphide (e.g., Sakai et al., 1982, 1984). According to Holloway and Blank (1994), the variations of $\delta^{34}S$ values resulted from continuous volatile exsolution can be modelled either as closed-system (Eq. 2) or as open-system (i.e., Rayleigh distillation) degassing (Eq. 3):

$$\delta^{34}S_f = \delta^{34}S_i + 1000\,(1 - F)\,\ln\ \alpha_{gas-melt} \quad (2)$$

$$\delta^{34}S_f = (\delta^{34}S_i + 1000)\,(F\alpha_{gas-melt}-1) - 1000 \quad (3)$$

where subscripts *f* and *i* refer to the final and initial isotopic compositions of S in the melt, respectively, *F* is a fraction of sulphur remaining in the melt upon degassing, and $\alpha_{gas-melt}$ is a gas-melt S-isotope fractionation factor defined as:

$$\alpha_{gas-melt} = (^{34}S/^{32}S)_{gas}/(^{34}S/^{32}S)_{melt} \quad (4)$$

To calculate the parameter *F* in Eqs. (2) and (3), we used S-concentrations in final ($[S]_f$) and initial ($[S]_i$) melts normalised to a concentration of an incompatible trace element (metal; $[Me]_f$ and $[Me]_i$, respectively) by the following equation:

$$F = ([S]_f \times [Me]_i)/([S]_i \times [Me]_f) \quad (5)$$

using, in particular, the concentrations of Ce and K in the respective melts, and then the average was used. Two melt inclusions with the highest S concentrations and $\delta^{34}S$ values (3/4-4-1 and 13/2-1-2, PEC- and exsolution-corrected values; Table S2.1 – Supporting online material) were taken to calculate the initial melt composition ($[S]_i$ = 3287 μg/g, $[Ce]_i$ = 9.54 μg/g, $[K]_i$ = 3592 μg/g, and $\delta^{34}S_i$ = + 11.2‰).

Modelling of S isotopic fractionation caused by degassing is rather complicated because $\alpha_{gas-melt}$ can be either higher or lower than unity because it depends strongly on *T*, fO_2 and the proportion of SO_4^{2-} and S^{2-} species dissolved in the melt. Generally, a fractionation factor of ^{32}S and ^{34}S isotopes between gas phase and silicate melt ($\Delta^{34}S_{gas-melt}$) can be expressed as following (e.g., Sakai et al., 1982), assuming that isotopic equilibrium is maintained among all sulphur species in the gaseous and melt phases:

$$\Delta^{34}S_{gas-melt} = \delta^{34}S_{gas} - \delta^{34}S_{melt} \approx 1000\ \ln\ \alpha_{gas-melt} = \\ = [X\delta^{34}S_{SO_2} + (1-X)\delta^{34}S_{H_2S}] - [Y\delta^{34}S_{sulfide} + (1-Y)\delta^{34}S_{sulfate}] \quad (6)$$

where *X* is the mole fraction of SO_2 in the SO_2-H_2S gas phase (i.e., $X_{SO_2} + X_{H_2S} = 1$), and *Y* is the mole fraction of sulphur dissolved in the melt as sulphide, and 1 − *Y* mole fraction of sulphur dissolved as sulphate. After multiplying and collecting terms, Eq. (6) can be expressed as:

$$1000\ \ln\ \alpha_{gas-melt} = X1000\ \ln\ \alpha_{SO_2-H_2S} + Y1000\ \ln\ \alpha_{sulphate-sulphide} - \\ -1000\ \ln\ \alpha_{sulphate-H_2S} \quad (7)$$

The temperature dependences of the fractionation factors in Eq. (7) can be approximated by the relationships studied by Richet et al. (1977)

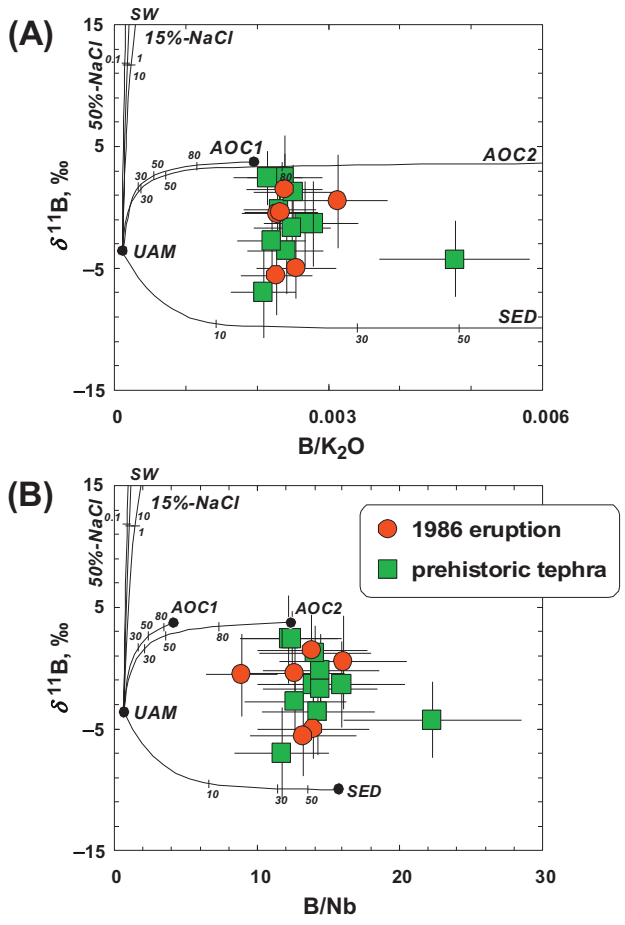

Fig. 8. Boron isotope composition of the studied glass inclusions given in relation to B/K_2O (A) and B/Nb (B) in context of possible magma contamination. The mixing end-members used (and their labels) are the same as in Fig. 7. It is demonstrated that magma contamination by seawater or seawater-derived components, altered oceanic crust and marine sediments is unable to account for B isotopic composition of the studied melt inclusions.

and Miyoshi et al. (1984) (for more detail, see a compilation by Taylor, 1986):

$$1000 \ln \alpha_{SO_2-H_2S} = -0.42 \times 10^9/T^3 + 4.367 \times 10^6/T^2 - 0.105 \times 10^3/T - 0.41 \quad (8)$$

$$1000 \ln \alpha_{sulphate-sulphide} = 7.4 \times 10^6/T^2 - 0.19 \quad (9)$$

$$1000 \ln \alpha_{sulphate} = 6.5 \times 10^6/T^2 \quad (10)$$

where T is temperature in Kelvin. For the temperature range from 910 to 1180 °C determined for the studied Chikurachki melt inclusions (Gurenko et al., 2005a), the $\Delta^{34}S_{gas-melt}$ fractionation factor is within the range of −2.1‰ to −0.9‰ (i.e., $\alpha_{gas-melt}$ = 0.9979–0.9991). The calculations were done assuming X = 0.98 because usually the volcanic gases emitted at temperatures ~1000 °C contain mostly SO_2, whereas H_2S is present only in trace amount, as shown for Kilauea volcano, Hawaii, and Mnt. Etna, Sicily (Symonds et al., 1994) and according to the recent gas-melt equilibria model of Burgisser and Scaillet (2007) for oxidised (i.e., ΔNNO = +1.5) conditions. The variations of X within ± 10% (from 0.8 to 1) will cause an uncertainty in the resulting $\Delta^{34}S_{gas-melt} \approx \pm$ 0.2–0.3‰. The Y value varied from 0.02 to 0.2, in agreement with the previously reported ΔNNO-range from +1 to +2, resulting in 80 to 98% sulphur dissolved as sulphate in the melt (see above).

The diagram of $\delta^{34}S$ versus F (Fig. 9) demonstrates that neither open- nor close-system degassing can account for the observed ~14‰ range in the Chikurachki melt inclusions. This is mostly because the outgassed SO_2 will preferentially drive out the lighter ^{32}S isotope under conditions of high fO_2 so that the remaining melt will be progressively enriched in ^{34}S, as it was first shown by Sakai et al. (1982) and also demonstrated by Mandeville et al. (2009) for the case of climatic and pre-climatic eruptions of Mt. Mazama, Crater Lake, Oregon, but being completely opposite to what is observed in Fig. 6A and Fig. 9. Negative correlations of S with incompatible trace elements mentioned above (Fig. 5B) may suggest that magma fractionation (resulting in enrichment of melt by incompatible trace elements) might have been accompanied by S-depletion due to degassing. However, a weak correlation of S with CO_2 and no correlations with other volatile components (like H_2O and Cl) imply that degassing, though being probably

Table 1
Composition of mixing end-members used for calculation of mixing lines illustrating magma contamination.

Component	Ce	Nb	Ba	Cl	B	H_2O	K_2O	$\delta^{11}B$
	μg/g	μg/g	μg/g	μg/g	μg/g	wt%	wt%	‰
UAM[a]	15.37	1.28	–	128.49	0.9	0.26	0.804	−3.7
SW[b]	1.20E–06	1.50E–05	–	19,350	4.5	97.5	0.048	39.5
15%-NaCl[c]	6.00E–06	7.94E–05	–	99,000	100	85	0.25	25.5
50%-NaCl[c]	2.00E–06	2.48E–04	–	303,000	312	50	0.78	56.6
AOC1[d]	6.01	1.22	–	2040	5.2	5	0.265	3.7
AOC2[d]	3.52	0.42	–	35	5.2	2.5	0.03	3.7
SED[e]	50.11	7.67	–	1000	120	10.1	1.7	−10
MW[f]	–	0.21	1.2	–	0.05	–	–	−4
SSF1[g]	–	0.474	10,861	–	300	–	–	15
SSF2[g]	–	0.375	2091	–	100	–	–	3
SSF3[g]	–	0.364	1117	–	50	–	–	−8

[a] UAM = "uncontaminated" arc magma. The concentrations of K_2O, Nb and Ce were defined as average of all melt inclusions (Table S2.1 – *Supporting online material*) using PEC-corrected concentrations, B content and $\delta^{11}B$ was taken from Chaussidon and Marty (1995), the concentrations of H_2O and Cl were calculated using those of neighbouring elements in the multi-element diagram (Fig. 3): $[H_2O]_n = ([Ce]_n \times [Pr]_n)^{0.5}$, $[Cl]_n = ([Nb]_n \times [K]_n)^{0.5}$.

[b] SW = seawater composition at 3.5% salinity. The elemental composition of SW was taken from Turekian (1968), B content and $\delta^{11}B$ is from Leeman and Sisson (1996).

[c] 15%- and 50%-NaCl brines with chemical and isotopic compositions as defined in Gurenko and Kamenetsky (2011).

[d] AOC = altered oceanic crust. The composition of AOC1 is from Gurenko and Kamenetsky (2011), and AOC2 (elemental composition) is from le Roux et al. (2006), except for B and $\delta^{11}B$ that are the same as in AOC1.

[e] SED = siliceous marine sediment with the concentrations of H_2O, K_2O, Nb and Ce as those in the Kurile arc sediment from Plank and Langmuir (1998), and of Cl, B and $\delta^{11}B$ from Gurenko and Kamenetsky (2011).

[f] MW = mantle wedge. The concentrations of trace element correspond to the depleted mantle after Salters and Stracke (2004), and B content and $\delta^{11}B$ was taken from Chaussidon and Marty (1995).

[g] SSF1 to SSF3 = subducting slab fluids (see text for more detail).

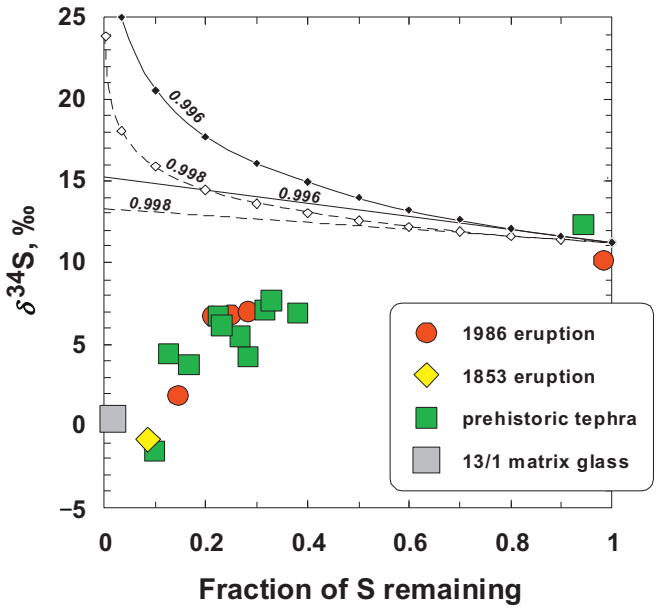

Fig. 9. Sulphur isotope fractionation during magma degassing. The $\delta^{34}S$ values in the melt inclusions are shown versus fraction of S remaining (*F*). Shifts of $\delta^{34}S$ were calculated assuming closed-system (equilibrium, solid and dashed *straight lines*) and open-system (Rayleigh distillation; solid and dashed *curves*) degassing (see text), the $\alpha_{gas-melt}$ values of 0.996 and 0.998, and maximum, undegassed S concentration found in the most S-rich melt inclusions having the highest $\delta^{34}S$ values. At the temperature range from 910 to 1180 °C and the redox conditions of NNO + 1 to NNO + 2 obtained for the studied Chikurachki magmas, the outgassed SO_2 will drive out the lighter ^{32}S isotope so that the remaining melt will be progressively enriched in ^{34}S. Thus, degassing alone cannot explain the observed, ~10‰-S-isotope of the studied melt inclusions.

important, was not a single process affecting the concentrations of the dissolved S. Furthermore, the fact that the hyperbola-shaped relationship of $\delta^{34}S$ vs. S concentrations (Fig. 6A) is transformable into a straight line in the 1/S-$\delta^{34}S$ space (Fig. 6B) represents a strong argument in favour of two-component mixing hypothesis (Langmuir et al., 1978), whereas host lapilli groundmass glasses, which presumably suffered degassing, do not fit the line. We thus contend that sulphur abundances, the entire S-isotope range, as well as the other volatile components such as H_2O, Cl and F correlating with each other (Fig. 5) were largely controlled by two-component mixing process. The possible mixing end-members could be the magmas having similar major and trace element compositions but strongly contrasting volatile contents and S isotopes.

5.3. Trace element constraints on magma source components

Mafic arc magmatism results from melting of a mantle wedge, whose solidus is lowered by input of slab-derived hydrous melts and/or fluids (e.g., Gill, 1981; McCulloch and Gamble, 1991; Hawkesworth et al., 1993; Woodhead et al., 1993; Pearce and Peate, 1995). The composition of the mantle wedge is relatively well constrained and thought to be represented by a MORB-type, or even more depleted upper mantle material (e.g., Woodhead et al., 1993; Kepezhinskas et al., 1997). However, a relative contribution of slab-derived H_2O-rich fluids and/or melts, as well as the proportion of the sediments relative to the mafic part of the oceanic crust in the slab remains enigmatic. Numerous previous studies attempted to assess the effect of fluid transport vs. slab melting in the origin of the Kurile-Kamchatka arc magmas (e.g., Hochstaedter et al., 1996; Ishikawa and Tera, 1997; Kepezhinskas et al., 1997; Khubunaya and Sobolev, 1998; Dorendorf et al., 2000; Churikova et al., 2001, 2007; Ishikawa et al., 2001; Portnyagin et al., 2007, 2015, Konrad-Schmolke et al., 2016, among others). One of the main purposes of the present study is to constrain a contribution of the above mentioned components to the origin of the Chikurachki magmas using the behaviour of fluid-immobile (i.e., Nb, Zr, Ti, Yb) vs. fluid-mobile (i.e., B, Ba, K, Sr, ± Th) elements.

5.3.1. Mantle wedge composition

In our model calculations, it is essential to assess chemical composition of the mantle wedge. Generally, the HFSE and HREE are immobile in the fluid and not enriched in the oceanic crust and in sedimentary components of the subduction slab, and the ratios of these elements can be used as reasonable proxy to characterise the nature of the mantle wedge of a particular volcano in the SZ setting (e.g., Pearce, 1983; Pearce and Peate, 1995).

Several trace element characteristics of the studied Chikurachki melt inclusions allow us to conclude that the composition of the mantle wedge is similar or even more depleted than the source of typical N-MORB magmas. They are following: (*i*) the average N-MORB-normalised concentrations of $[Nb]_n = 0.55 \pm 0.21$, $[Sm]_n = 1.16 \pm 0.37$, $[Zr]_n = 0.74 \pm 0.30$, $[Ti]_n = 0.74 \pm 0.27$, $[Yb]_n = 0.83 \pm 0.29$ are close to, or lower, than unity; (*ii*) the element ratios Zr/Nb = 35–49, Zr/Yb = 16–25, and Nb/Yb = 0.35–0.7 are similar to those of N-MORB (i.e., Zr/Nb = 32, Zr/Yb = 24, Nb/Yb = 0.76; Hofmann, 1988); (*iii*) the studied melt inclusions plot in the field of MORB in the Pearce and Peate (1995) Zr/Yb vs. Nb/Yb discrimination diagram (not shown). Thus, to simplify our calculations, we assume the trace element concentrations of the Kurile arc mantle wedge is the same as depleted N-MORB mantle of Salters and Stracke (2004) (Table 1). We note that using more depleted composition of the mantle wedge will not significantly change the calculation results, but slightly increase a role of the slab-derived components.

5.3.2. Subduction slab melt vs. fluid as a volatile transport media

The origin of arc magmas is tightly related to dehydration and/or melting of the slab, where both melt and fluid components are added in different proportions, namely higher proportion of fluid at shallower depths and *vice versa* when the slab penetrates deeper (Hickey and Frey, 1982; Cameron, 1985; Tatsumi et al., 1986; Crawford et al., 1989; Elliott et al., 1997). Experiments on element partitioning confirm that slab-derived H_2O-rich fluids may cause remarkable enrichment by incompatible elements typical for volcanic arcs worldwide (e.g., Brenan et al., 1995; Ayers et al., 1997; Stalder et al., 1998; Johnson and Plank, 1999). Silica-rich partial melts released from the subducting crust and/or sediment are also potential contributors to the chemical balance (Defant and Drummond, 1990; Drummond and Defant, 1990).

Several studies proposed a concurrent addition of slab-derived melt and fluid components in the arc magmas (e.g., Kay, 1978; Rogers et al., 1985; Stern et al., 1984; Defant et al., 1991; Stern and Kilian, 1996; Class et al., 2000; Yogodzinski et al., 2001). In particular, it has been concluded that hydrous fluids released in the arc front due to amphibole and serpentine dehydration are enriched in boron, LILE, sulphur and chlorine and likely represent a main fluid transport and reaction agent affecting mantle wedge of the Kurile and Kamchatka arcs (e.g., Hochstaedter et al., 1996; Ishikawa and Tera, 1997; Churikova et al., 2001, 2007; Portnyagin et al., 2007). Moreover, Churikova et al. (2007) concluded that S, Cl and B could have been transported by a fluid released from *AOC*-like subduction slab at shallow depth, whereas Li appeared to be related to Li-F-rich fluids resulting from breakdown of volatile-rich minerals (e.g., amphibole) at much greater depths (~400 km). Furthermore, Churikova et al. (2007) have noted that some Kurile-Kamchatka arc magmas may also exhibit an adakitic signature, whereas Portnyagin et al. (2015) argued that melting of the mantle wedge beneath Tolbachik was triggered by slab-derived hydrous melts.

We think that in the case of Chikurachki, the significant positive correlations of H_2O/K_2O vs. Cl/K_2O and F/Zr vs. Cl/Nb (Fig. 5E,F), Th/Nb vs. Ba/Nb ($R = 0.65$; see Fig. 9 and discussion below), as well as B/Nb vs. Li/Nb and Be/Nb ($R = 0.83$ and 0.80, respectively, except for one outlier; Fig. S2.3 – Supporting online material) imply a complex

nature of the Kurile arc subduction component composed of both melt and fluid. The observed strong correlations of Li/Nb and Be/Nb with B/Nb and F/Zr with Cl/Nb in the Chikurachki melt inclusions suggest that these elements have a common source (i.e., slab component), support a major role of a Cl-rich fluid and imply that B, Cl and F are likely to relate to a single transport process, in contrast to the mechanism of B and Li decoupling suggested by Churikova et al. (2007).

5.3.3. Trace element constraints

Thorium and LREE are enriched in the subducted slab, being however less mobile or nearly immobile in the fluid phase, as compared to fluid-mobile elements, such as Li, B, Ba, Pb and Sr. The difference in geochemical behaviour of these elements can be used to elucidate a contribution of slab-derived melts vs. dehydration fluids in the origin of arc magmas (e.g., Kamenetsky et al., 1997; Class et al., 2000; Hochstaedter et al., 2001). Namely, the transport by fluid would leave Th/Nb ratios virtually unchanged since both elements are immobile, but affect the ratios of fluid-mobile to fluid-immobile elements (e.g., Ba/Nb, B/Nb), and *vice versa*, if the element transport would have been caused solely by the slab-derived melt. Systematic variations of Th/Nb vs. Ba/Nb or B/Nb ratios would imply the contribution of both slab-derived melt and fluid components.

We modelled the contribution of the anticipated subduction sediment-derived melt and fluid components to the mantle wedge following the approach of Hochstaedter et al. (2001). The *AOC*- and *SED*-derived fluids, as well as a partial melt from *SED* were considered as possible end-members (Table 2). The element partitioning data used in the modelling are from experimentally-determined bulk sediment-melt, sediment-fluid, rutile-melt and rutile-fluid partition coefficients (Brenan et al., 1994, 1995; Stalder et al., 1998; Johnson and Plank, 1999; Foley et al., 2000). The sediment subducted at the Kurile trench (its composition is taken from Plank and Langmuir, 1998) is thought to contain up to 5% Ti-rich residual phase (i.e. rutile), which has the potential to fractionate Nb from Th (Class et al., 2000), whereas 1% rutile was assigned for *AOC* (Hochstaedter et al., 2001). Equilibrium batch melting and Rayleigh fractionation equations (Shaw, 1970) were used to calculate the compositions of partial melt and fluid in equilibrium with the subduction sediment, respectively. We assumed 5% partial melting of the Kurile sediment to produce a sediment melt mixing end-member, and 2% fluid removal from both the Kurile sediment and *AOC* to account for a possible sediment fluid end-member (Fig. 10). We note also that because Ba, Nb and Th are chemical elements of very similar incompatibility to minerals composing magma source rocks, as follows from their solid-melt partition coefficients, they show little or no fractionation during partial melting and/or magma fractionation. The calculated Ba/Nb and Th/Nb ratios of the multi-

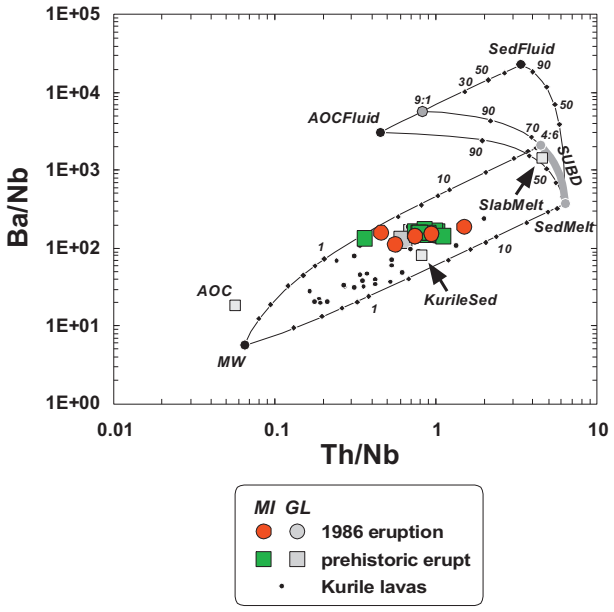

Fig. 10. Diagram Th/Nb vs. Ba/Nb illustrating a possible origin of the Chikurachki magmas as a result of melting of a three-component magma source. Legend: *MI* = melt inclusions, *GL* = matrix glasses. The source components are mantle wedge (*MW*) with Ba, Nb and Th concentrations of the depleted mantle after Salters and Stracke (2004) and hybrid subduction component (*SUBD*) representing a binary 4:6-mixture of a sediment melt (*SedMelt*) with a composite slab-derived fluid, which in turn is a 9:1-mixture of a dehydration fluids released from the altered oceanic crust (*AOCFluid*) and Kurile sediment (*SedFluid*) (see text and Table 2 for definition). The compositions of *Kurile lavas* are from Bailey et al. (1987a, 1987b), Ishikawa and Tera (1997), Ikeda (1998), Ikeda et al. (2000), Takagi et al. (1999), Ishikawa et al. (2001). *KurileSed* is a bulk composition of the sediment column subducted at the Kurile trench taken from Plank and Langmuir (1998). *AOC* is altered oceanic crust taken from Staudigel et al. (1996), whose composition was used by Hochstaedter et al. (2001) to calculate *AOCFluid* composition. *SlabMelt* is a composition of composite hydrous melt released from the slab and contributed to the origin of magmas erupted in the Tolbachik volcanic field, Kamchatka, which was taken from Portnyagin et al. (2015) for comparison.

Table 2
Trace element compositions of mixing end-members and bulk distribution coefficients used in calculations of composite magma source[a].

Component	MW[b]	Kurule	Sed	Sed	AOC[e]	AOC	SUBD[g]	Slab	$D_{sed\text{-}melt}$[i]	$D_{rut\text{-}melt}$[i]	$D_{sed\text{-}fluid}$[i]	$D_{rut\text{-}fluid}$[i]
		Sed[c]	Melt[d]	Fluid[d]		Fluid[f]		Melt[h]				
Ba	1.2	627	410	10,861	22.6	1117	1419	310	1.64	0.01	0.05	0
Nb	0.21	7.67	1.12	0.47	1.22	0.36	0.67	0.22	1.21	119	2.99	271
Th	0.014	6.22	7.08	1.6	0.07	0.17	3.02	1.00	0.89	0.54	4.13	0.05
Ba/Nb	5.71	81.7	366	23,109	18.5	3103	2118	1409	–	–	–	–
Th/Nb	0.067	0.81	6.32	3.4	0.057	0.47	4.51	4.55	–	–	–	–

[a] Element concentrations are given in ppm; – = no value.
[b] *MW* = mantle wedge with trace element concentrations of the depleted mantle after Salters and Stracke (2004).
[c] *KurileSed* = bulk composition of sediment column subducted at the Kurile trench from Plank and Langmuir (1998).
[d] *SedMelt* and *SedFluid* are melt and fluid compositions, respectively, derived from the composition of Kurile sediment containing 5% residual rutile. *SedMelt* represents a liquid resulted from 5% batch melting of the Kurile sediment, whereas *SedFluid* was calculated assuming 2% of aggregate fluid removal in accordance with Rayleigh's fractionation model (Shaw, 1970), using bulk partition coefficients listed here (see below for explanation).
[e] *AOC* = altered oceanic crust taken from Staudigel et al. (1996), whose composition was used by Hochstaedter et al. (2001) to calculate AOC-derived fluid composition.
[f] *AOCFluid* = fluid released by dehydration of AOC from Hochstaedter et al. (2001).
[g] SUBD = subduction component obtained during the present study to account for the composition of Chikurachki melt inclusions. SUBD ranges in composition from the pure *SedMelt* component (presenting a lower limit of the range) to that representing a 4:6-mixture of *SedMelt* component with a composite slab-derived fluid, which in turn represents a 9:1-mixture of *AOCFluid* and *SedFluid* components (upper limit of the range) listed in this column.
[h] *SlabMelt* = composite water-bearing slab melt contributed to the origin of magmas erupted in the Tolbachik volcanic field, Kamchatka (Portnyagin et al., 2015).
[i] Bulk $D_{sed\text{-}melt}$ = sediment-melt, $D_{rut\text{-}melt}$ = rutile-melt, $D_{sed\text{-}fluid}$ = sediment-fluid, and $D_{rut\text{-}fluid}$ = rutile-fluid partition coefficients adopted from Brenan et al. (1994, 1995), Stalder et al. (1998), Johnson and Plank (1999), Foley et al. (2000).

component magma source region are thus relevant for the Th/Nb and Ba/Nb of the produced partial melts, and can be used to assess the origin of the Chikurachki parental magmas.

In the model presented in Fig. 10, the Th/Nb vs. Ba/Nb variations observed in the Chikurachki melt inclusions (presented alongside whole-rock chemical compositions of the Kurile arc mafic lavas) can be explained by partial melting of a magma source composed of the following three components (Table 2):

1. A mantle wedge (*MW*) component with trace element concentrations of depleted mantle after Salters and Stracke (2004).
2. A composite dehydration fluid, which is enriched in Ba relative to Th or Nb and presents a 9:1 mixture of the fluid released from the altered oceanic crust (*AOCFluid*, the composition is taken from Hochstaedter et al., 2001) and a fluid produced by dehydration of a subduction sediment (*SedFluid*), whose trace element composition was calculated from that of the Kurile sediment after Plank and Langmuir (1998) (for more detail, see explanatory notes in Table 2). The 9:1 proportion of *AOCFluid* to *SedFluid* was selected arbitrary, given a subordinate amount of the sediment relative to a total mass of the slab, taking also into account that sediment is more volatile-rich, as compared to its basaltic and ultramafic counterparts. We note however that variations of *AOCFluid* to *SedFluid* ratio do not affect significantly the calculation results.
3. A sediment-derived melt (*SedMelt*) with slightly elevated Th/Nb ratios and significantly lower Ba/Nb ratios, as compared *AOCFluid* and *SedFluid* mixing end-members, whose trace element composition was also calculated from the composition of the Kurile sediment (see also explanatory notes in Table 2).

As it follows from our calculations, the composition of subduction component (*SUBD*) is variable. It ranges from the composition of the pure *SedMelt* component (representing a lower limit of the range) to that of *SedMelt* mixed with up to 60% composite slab-derived fluid presenting, in turn, a 9:1-mixture of *AOCFluid* and *SedFluid*, crudely corresponding to the *AOC* to *SED* proportion in the dehydrating model slab (Tonarini et al., 2011) and assuming also equal amount of fluid released from both lithologies. The ~1–8% admixture of *SUBD* to *MW* appeared to satisfactorily explain the entire compositional range of the Chikurachki melt inclusions, and from ~0.4% to ~10% of *SUBD* to be mixed with *MW* to account for the range of the Kurile arc magmas (Fig. 10). In conclusion, it is worth emphasising that the subduction component contributed to the origin of the Tolbachik magmas (Portnyagin et al., 2015) appeared to be very similar to *SUBD* inferred during the present study (Fig. 9; Table 2).

5.3.4. Implications for chemical composition and amount of slab-derived fluid

Here we evaluate a possible contribution of slab-derived fluid to the origin of volatile components and boron in the studied magmas, assessing the observed B-isotope range. The light lithophile element boron is a powerful proxy to trace fluid transport of chemical elements from subducting slab to the mantle wedge because of strongly contrasting B concentrations and δ^{11}B values in these geochemical reservoirs. A significant fraction of initial boron is contained in the uppermost few km of the subducting crust and sediments, being then progressively released as subduction proceeds (e.g., Leeman and Sisson, 1996). Systematically higher δ^{11}B values in the volcanic arc magmas, as compared to the exhumed subduction-related metamorphic rocks, suggest that dehydration reactions cause significant decrease of δ^{11}B values of subducted crustal material, implying strong fractionation of ^{10}B and ^{11}B isotopes as boron partitions in the fluid (e.g., Peacock and Hervig, 1999). This conclusion was supported by later experimental study of Wunder et al. (2005), who have demonstrated that a wide range of δ^{11}B in the arc magmas may result from continuous breakdown of micas, if they are present in the down-dragged slab. Finally, a

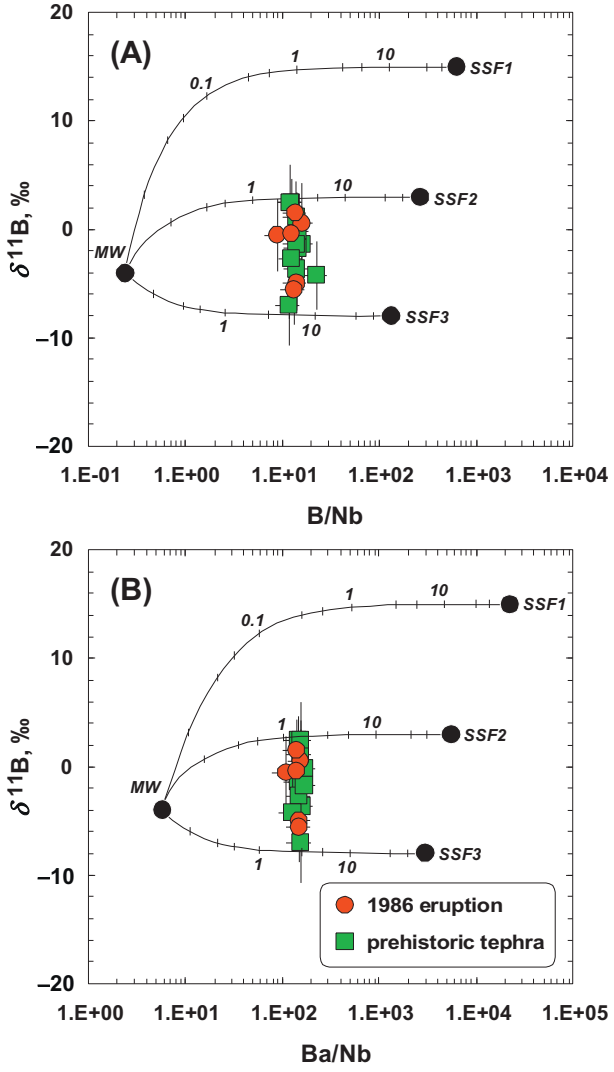

Fig. 11. Diagrams of (A) δ^{11}B vs. B/Nb and (B) δ^{11}B vs. Ba/Nb illustrate the proposed interpretation to account for B-isotope variations in the Chikurachki mineral-hosted melt inclusions by addition of slab-derived fluids to the mantle wedge. Mixing lines between the depleted MORB-type mantle wedge (*MW*) and subduction slab fluids (*SSF1*, *SSF2* and *SSF3*) are shown (see Table 1 for chemical composition). Numbers on mixing lines refer to wt% of component added to MW end-member.

serpentinised mantle wedge at the slab-mantle interface represents another major inventory of boron, being also a source of variable but generally positive δ^{11}B values (e.g., Benton et al., 2001; Straub and Layne, 2002; Savov et al., 2005, 2007; Scambelluri and Tonarini, 2012).

Boron mobilised from the slab was shown to be systematically enriched in ^{11}B than the parental *AOC* at 400–500 °C, resulting in + 5 to + 10‰ enrichment of the fluid relative to the solid (Ishikawa and Nakamura, 1992; Leeman and Sisson, 1996; Rose et al., 2001; Rosner et al., 2003; Leeman et al., 2004; Le Voyer et al., 2008). Since the composition of slab-derived fluid may vary strongly, depending on the composition of subducting crust and the degree of its devolatilisation, a wide δ^{11}B range from − 7‰ up to + 15‰ (assuming + 10‰ enrichment of the fluid phase relative to the upper end of the δ^{11}B range given for *AOC* by Smith et al., 1997) is very probable (Rose et al., 2001; Leeman et al., 2004; Gurenko et al., 2005b; Le Voyer et al., 2008; Tonarini et al., 2011; Scambelluri and Tonarini, 2012).

The effects of possible interaction of slab-derived fluids with depleted MORB-like mantle source are illustrated in diagrams in coordinates of δ^{11}B vs. B/Nb and Ba/Nb ratios (Fig. 11). Given the

$^{11}B/^{10}B$, B/Nb and Ba/Nb do not change significantly during partial melting or magma fractionation, these ratios, being calculated for the magma source, can be directly transferred to the resulting partial melts. The following mixing end-members were defined (Table 1):

1. Mantle wedge (*MW*) was chosen to contain 1.2 μg/g Ba, 0.21 μg/g Nb, 0.06 μg/g B and $\delta^{11}B = -4$‰ (Chaussidon and Marty, 1995; Salters and Stracke, 2004).
2. Subducting slab fluid (*SSF*) varies significantly in chemical composition, depending on the particular chemical and lithological composition of the slab and the dehydration depth. In particular, Tonarini et al. (2011) have demonstrated that slab-derived fluids released at the depth range from 30 to 120 km may contain from ~10 and ~200 μg/g B and vary between −10 to higher than +20‰ $\delta^{11}B$. Three contrasting fluid compositions (*SSF1* through *SSF3*) were compiled based on the data of Hochstaedter et al. (2001), Rose et al. (2001), Straub and Layne (2002), Rosner et al. (2003), Leeman et al. (2004), Gurenko et al. (2005b), Le Voyer et al. (2008), Tonarini et al. (2011), Scambelluri and Tonarini (2012), using also the compositions of *SED* and *AOC*-derived fluids calculated during the present study (*SSF1*: trace elements concentrations are those as of *SEDFluid*, containing 300 μg/g B and $\delta^{11}B = +15$‰; *SSF2* is the 9:1 mixture of *AOCFluid* and *SedFluid* as calculated above, containing 100 μg/g B and $\delta^{11}B = +3$‰; and *SSF3* is equal to *AOCFluid* with 50 μg/g B and $\delta^{11}B = -8$‰). The decrease of B and Ba contents and $\delta^{11}B$ values in the fluid components qualitatively reflects the increase of slab temperature and degree of its devolatilisation.

As it follows from the calculations, the slab-derived fluid may represent a major agent affecting the abundances of volatile and fluid-mobile elements, and B isotopes in the melt inclusions. About 1–10% of *SSF2* and *SSF3* have to be added to *MW* in order to explain the ~9‰ range of $\delta^{11}B$ values of the studied melt inclusions. We note that this estimation is very similar to that inferred from the trace element modelling (1 to 8% addition of *SUBD*; Fig. 9). It is also worth emphasising that the selected compositions of *SSF2* and *SSF3* are very close to the model fluid compositions released from the South Sandwich Island arc uppermost slab at 90–120 km depth (170–190 μg/g B and $\delta^{11}B = -0.7$ to −3.9‰; Tonarini et al., 2011), but having less boron and more negative $\delta^{11}B$ values. This discrepancy can be explained by stronger dehydration of the residual Kurile slab because of the greater depth of the Wadati-Benioff zone beneath Chikurachki (~130–140 km; e.g., Ishikawa and Tera, 1997; Ishikawa et al., 2001).

5.4. Magma ascent, degassing history and eruption style

It is well known that conduit geometry, magma viscosity, degassing history, changing conditions of magma ascent and fragmentation, and even the dynamics of *syn*-eruptive microlite growth may strongly affect the eruption rate and style of a volcano (e.g., Fisher and Schmincke, 1984; Carey and Sparks, 1986; Houghton et al., 2004; Szramek et al., 2006, 2010; Houghton and Gonnermann, 2008). Previously, Gurenko et al. (2005a) suggested intensive pre-eruptive degassing of H_2O and S from the magma at the stage of phenocryst crystallisation, pointing on the strongly varying to very low volatile contents in the melt inclusions trapped by phenocrysts of the same or very close chemical composition. The authors suggested a scenario, by which local volumes of magma could be partially degassed before being trapped by growing crystals, and employed a mechanism of vertical cycling of magma within one or between several connected reservoirs, being akin to the magma drain-back phenomenon described in particular for Kilauea Volcano, Hawaii (e.g., Wallace and Anderson, 1998). Our present data (i.e., numerous correlations of volatile component concentrations and S isotope compositions preserved in the studied melt inclusions with incompatible trace elements and between each other, inability of magma degassing and crustal contamination to account for these variations coupled with the suggested here two-component mixing scenario to explain $\delta^{34}S$ vs. S concentrations) could be interpreted in support of the mechanism previously suggested by Gurenko et al. (2005a) to control the variations of H_2O, S, Cl and F in the erupting magmas.

The required insignificant correction of melt inclusion compositions for post-entrapment crystallisation of host mineral (i.e., < 7.8 wt% Ol, 0.8 wt% Opx, and no correction for Pl) also suggests that the eruption and quenching of magma likely occurred shortly after the inclusions have been entrapped by growing phenocrysts. As previously discussed (e.g., Roggensack et al., 1997; Gurenko et al., 2005a; Shinohara, 2008; Ruth et al., 2016), eventual eruptions may be non-explosive, if magma degassing is effective at shallow crustal depth, whereas rapid ascent of a volatile-rich magma may result in strong volatile release and highly explosive character of eruptions. In this context, the range of volatile contents recorded by melt inclusions and their relationships with other chemical components may indicate whether the erupted magma underwent a prolonged stage of relatively passive degassing or degassing was essentially a single-stage process upon the eruption. It is worth emphasising that most of the historic eruptions from Chikurachki have been of the non-explosive character, possibly linked to the episodes where volatile components were able to dissipate smoothly. Explosive eruptions, in contrast, are thought to occur when access to shallow levels is blocked or when the flux of magma from depth is too rapid for shallow degassing to prevent a catastrophic decompression and explosive fragmentation of the magma. We thus think that rapid ascent of the volatile-rich basaltic magmas from ~16-km initial depth (inferred from our CO_2-H_2O data; Fig. 4B) was a primary reason caused the Plinian character of the Chikurachki eruptions.

6. Summary and conclusions

The present study focuses on the unravelling the origin and behaviour of volatile components resulting in highly explosive (Plinian) basaltic eruptions of the Chikurachki volcano. The following main conclusions were derived:

1. The obtained concentrations of volatile components in the studied melt inclusions agree well with our previously reported data. After correction for post-entrapment crystallisation of the host mineral, the concentrations of CO_2 and H_2O reveal minimum pressure of 33 to 276 MPa (or ~9.5 to ~1 km depth), corresponding to the last equilibrium between melt and vapour phases upon magma eruption and quenching. About 5–69% of the original CO_2 and 0.1–3.2% of H_2O were lost to the shrinkage bubble of melt inclusions after their entrapment during phenocryst crystallisation. After correction, the obtained 47–1580 μg/g CO_2, 0.4–4.2 wt% H_2O, 399–633 μg/g F, 619–3402 μg/g S and 805–1240 μg/g Cl ranges imply strong pressure release from 456 to 35 MPa, corresponding to ~15.7–1.2-km-depth range of magma ascent.
2. Significant negative correlations of S with incompatible trace elements, no clear relationships of S with H_2O, CO_2 and Cl but strong positive correlations of S/K_2O with H_2O/K_2O, Cl/K_2O and F/K_2O suggest that later magma degassing and/or contamination by crustal rocks were not the governing processes affecting the amounts of S and probably of the other volatile components preserved in inclusions.
3. Sulphur isotopes in the studied inclusion and groundmass glasses vary strongly, ranging from −1.6 to +12.3‰ of $\delta^{34}S$, decrease with decreasing S concentrations and show significant positive correlations with H_2O, CO_2 and S, as well as negative correlations with light lithophile (Li, Be and B), and with a number of incompatible trace elements. Our modelling has demonstrated that either open- or close-system magma degassing cannot account for the observed ~14‰ range of $\delta^{34}S$ variations in the Chikurachki melt inclusions. The linear character of the 1/S vs. $\delta^{34}S$ relationship

suggests mixing of two components possibly represented by melts having similar major and trace element compositions, but strongly contrasting volatile contents and S isotopes.

4. The $\delta^{11}B$ values of the studied melt inclusions range from −7.0 to +2.4‰ within the interval of B concentrations of 13–23 μg/g. Similarly, the relationships of $\delta^{11}B$ with B/K_2O and B/Nb, as well as of Cl/K_2O with B/K_2O (and equally, Cl/Nb with B/Nb) cannot be accounted by magma contamination at shallow crustal depths.
5. The observed relationships of S/K_2O with K_2O-normalised concentrations of H_2O, Cl and F, as well as the H_2O/K_2O vs. Cl/K_2O and F/Zr vs. Cl/Nb correlations strongly suggest that variations in H_2O, S, Cl and F contents were not primarily affected by degassing or contamination, but likely originated due to the mixing of magmas, which in turn reflect the composition of source components. We contend that subduction slab-derived melt and/or fluid were major agents in controlling chemical and isotopic composition of the mantle wedge and, consequently, of the magmas originated from this hybrid source.
6. The behaviour of fluid-mobile vs. fluid-immobile incompatible trace elements points towards strongly varying chemical composition of the subduction component. It ranges from the composition of the pure subducted sediment-derived melt (a lower limit of the range) to that of the sediment melt mixed with up to 60% composite slab-derived fluid, representing in turn a 9:1-mixture of fluid components released from both altered oceanic crust and the sediment of the slab. The ~1–8% admixture of the inferred subduction component to the mantle wedge is required to account for the whole compositional range of the studied Chikurachki magmas, and addition from ~0.4% to ~10% of the subduction component accounts for the broad compositional range of the Kurile arc magmas.
7. We conclude that rapid ascent of the volatile-rich basaltic magmas from ~16-km initial depth without their prolonged stagnation and crystallisation in shallower depth magma reservoir but accompanied by near-surface bubble nucleation and growth followed by magma fragmentation was a primary reason caused Plinian character of the Chikurachki eruptions.

Acknowledgements

We thank Peter Landry for his help and ensuring stable working conditions of the NENIMF CAMECA IMS 1280 instrument, Charlie Mandeville and Alberto Saal for fruitful discussions, Anastassia Borisova for review and comments of the early manuscript version. The insightful reviews, useful comments and suggestions, as well as a thorough correction of English by John Caulfield, Marco Fiorentini and one anonymous referee are very much appreciated. Editorial handling of the paper by Kate Kiseeva and Klaus Mezger is gratefully acknowledged. This work was benefited from the NENIMF financial support of AAG during his training as a SIMS research specialist, the NSF grant EAR 0911093 to AAG, and partially from the Russian Science Foundation grant #16-17-10145 to VSK and MEZ. This is CRPG contribution #2543.

Appendix A. Supplementary data

Supplementary data to this article can be found online at https://doi.org/10.1016/j.chemgeo.2017.10.009.

References

Alt, J.C., Shanks III, W.C., Jackson, M.C., 1993. Cycling of sulfur in subduction zones: the geochemistry of sulfur in the Mariana Island Arc and back-arc trough. Earth Planet. Sci. Lett. 119, 477–494.
Anderson, A.T., 1974. Chlorine, sulfur and water in magmas and oceans. Bull. Geol. Soc. Am. 85, 1485–1492.
Aster, E.M., Wallace, P.J., Moore, L.R., Watkins, J., Gazel, E., Bodnar, R.J., 2016. Reconstructing CO_2 concentrations in basaltic melt inclusions using Raman analysis of vapor bubbles. J. Volcanol. Geotherm. Res. 323, 148–162.
Ayers, J.C., Dittmer, S.K., Layne, G., 1997. Partitioning of elements between peridotite and H_2O at 2.0–3.0 GPa and 900–1100 °C, and application to models of subduction zone processes. Earth Planet. Sci. Lett. 150, 381–398.
Bailey, J.C., Frolova, T.I., Burikova, I.A., 1987a. Mineralogy, geochemistry and petrogenesis of Kurile Island Arc basalts. Contrib. Mineral. Petrol. 102, 265–280.
Bailey, J.C., Larsen, O., Frolova, T.I., 1987b. Strontium isotope variations in lower Tertiary-Quaternary volcanic rocks from the Kurile Island Arc. Contrib. Mineral. Petrol. 95, 155–165.
Belousov, A.B., Belousova, M.G., Grushin, S. Yu, Krestov, P.B., 2003. Historic eruptions of the Chikurachki volcano (Paramushir, Kuril Islands). Volcanol. Seismol. 3, 15–34 (in Russian).
Belousov, A., Belousova, M., Edwards, B., Volynets, A., Melnikov, D., 2015. Overview of the precursors and dynamics of the 2012–13 basaltic fissure eruption of Tolbachik volcano, Kamchatka, Russia. J. Volcanol. Geotherm. Res. 307, 22–37.
Belousov, A., Belousova, M., Kozlov, D., 2017. The distribution of tephra deposits and reconstructing the parameters of 1973 eruption on Tyatya Volcano, Kunashir I., Kuril Islands. Volcanol. Seismol. 11, 285–294.
Benton, L.D., Ryan, J.G., Tera, F., 2001. Boron isotope systematics of slab fluids as inferred from a serpentine seamount, Mariana forearc. Earth Planet. Sci. Lett. 187, 273–282.
Bernard, A., Demaiffe, D., Mattielli, N., Punanongbayan, R.S., 1991. Anhydrite-bearing pumices from Mount Pinatubo: further evidence for the existence of sulfur-rich silicic magmas. Nature 354, 139–140.
Bindeman, I.N., Ponomareva, V.V., Bailey, J.C., Valley, J.W., 2004. Volcanic arc of Kamchatka: a province with high-$\delta^{18}O$ magma sources and large-scale $^{18}O/^{16}O$ depletion of the upper crust. Geochim. Cosmochim. Acta 68, 841–865.
Brasseur, G., Granier, C., 1992. Mount Pinatubo aerosols, chlorofluorocarbons and ozone depletion. Science 257, 1239–1242.
Brenan, J.M., Shaw, H.F., Phinney, D.L., Ryerson, F.J., 1994. Rutile-aqueous fluid partitioning of Nb, Ta, Hf, Zr, U and Th: implications for high field strength element depletions in island-arc basalts. Earth Planet. Sci. Lett. 128, 327–339.
Brenan, J.M., Shaw, H.F., Ryerson, F.J., Phinney, D.L., 1995. Mineral-aqueous fluid partitioning of trace elements at 900 °C and 2.0 GPa: constraints on the trace element chemistry of mantle and deep crustal fluids. Geochim. Cosmochim. Acta 59, 3331–3350.
Burgisser, A., Scaillet, B., 2007. Redox evolution of a degassing magma rising to the surface. Nature 445, 194–197.
Cabral, R.A., Jackson, M.G., Koga, K.T., Rose-Koga, E.F., Hauri, E.H., Whitehouse, M.J., Price, A.A., Day, J.M.D., Shimizu, N., Kelley, K.A., 2014. Volatile cycling of H_2O, CO_2, F, and Cl in the HIMU mantle: a new window provided by melt inclusions from oceanic hot spot lavas at Mangaia, Cook Islands. Geochem. Geophys. Geosyst. 15, 4445–4467.
Cameron, W.E., 1985. Petrology and origin of primitive lavas from the Troodos ophiolite, Cyprus. Contrib. Mineral. Petrol. 89, 239–255.
Canil, D., Fellows, S.A., 2017. Sulphide–sulphate stability and melting in subducted sediment and its role in arc mantle redox and chalcophile cycling in space and time. Earth Planet. Sci. Lett. 470, 73–86.
Carey, S., Sparks, R.S.J., 1986. Quantitative models of the fallout and dispersal of tephra from volcanic eruption columns. Bull. Volcanol. 48, 109–125.
Carroll, M.R., Rutherford, M.J., 1985. Sulfide and sulfate saturation in hydrous silicate melts. J. Geophys. Res. 90, C601–C612.
Carroll, M.R., Rutherford, M.J., 1987. The stability of igneous anhydrite: experimental results and implications for sulfur behavior in the 1982 El Chichon trachyandesite and other evolved magmas. J. Petrol. 28, 781–801.
Carroll, M.R., Rutherford, M.J., 1988. Sulfur speciation in hydrous experimental glasses of varying oxidation state: results from measured wavelength shifts of sulfur X-ray. Am. Mineral. 73, 845–849.
Carroll, M.R., Webster, J.D., 1994. Solubilities of sulfur, noble gases, nitrogen, chlorine, and fluorine in magmas. In: Carroll, M.R., Holloway, J.R. (Eds.), Volatiles in Magmas. Reviews in Mineralogy, vol. 30. Mineralogical Society of America, Washington DC, pp. 231–279.
Caulfield, J.T., Cronin, S.J., Turner, S.P., Cooper, L.B., 2011. Mafic Plinian volcanism and ignimbrite emplacement at Tofua volcano, Tonga. Bull. Volcanol. 73, 1259–1277.
Chaussidon, M., Jambon, A., 1994. Boron content and isotopic composition of oceanic basalts: geochemical and cosmochemical implications. Earth Planet. Sci. Lett. 121, 277–291.
Chaussidon, M., Marty, B., 1995. Primitive boron isotope composition of the mantle. Science 269, 383–386.
Chaussidon, M., Albarède, F., Sheppard, S.M.F., 1987. Sulphur isotope heterogeneity in the mantle from ion microprobe measurements of sulphide inclusions in diamonds. Nature 330, 242–244.
Churikova, T., Dorendorf, F., Wörner, G., 2001. Sources and fluids in the mantle wedge below Kamchatka, evidence from across-arc geochemical variation. J. Petrol. 42, 1567–1593.
Churikova, T., Wörner, G., Mironov, N., Kronz, A., 2007. Volatile (S, Cl and F) and fluid mobile trace element compositions in melt inclusions: implications for variable fluid sources across the Kamchatka arc. Contrib. Mineral. Petrol. 154, 217–239.
Class, C., Miller, D.M., Goldstein, S.L., Langmuir, C.H., 2000. Distinguishing melt and fluid subduction components in Umnak Volcanics, Aleutian Arc. Geochem. Geophys. Geosyst. 1 (1999GC000010).
Connolly, J.W.D., Haughton, D.R., 1972. The valence of sulfur in glass of basaltic composition formed under low oxidation potential. Am. Mineral. 57, 1515–1517.
Crawford, A.J., Falloon, T.J., Green, D.H., 1989. Classification, petrogenesis and tectonic setting of boninites. In: Crawford, A.J. (Ed.), Boninites. Unwin Hyman, London, pp. 1–49.

Dalou, C., Koga, K.T., Le Voyer, M., Shimizu, N., 2014. Contrasting partition behaviour of F and Cl during hydrous mantle melting: implications for Cl/F signature in arc magmas. Prog. Earth Planet. Sci. 1, 26.
Davidson, J.P., 1987. Crustal contamination versus subduction zone enrichment: examples from the Lesser Antilles and implications for mantle source composition of island arc volcanic rocks. Geochim. Cosmochim. Acta 51, 2185–2198.
Defant, M.J., Drummond, M.S., 1990. Derivation of some modern arc magmas by melting of young subducted lithosphere. Nature 347, 662–665.
Defant, M.J., Richerson, P.M., De Boer, J.Z., Stewart, R.H., Maury, R.C., Bellon, H., Drummond, M.S., Feigenson, M.D., Jackson, T.E., 1991. Dacite genesis via both slab melting and differentiation: petrogenesis of La Yeguada volcanic complex, Panama. J. Petrol. 32, 1101–1142.
Ding, T., Valkiers, S., Kipphardt, H., De Bièvre, P., Taylor, P.D.P., Gonfiantini, R., Krouse, R., 2001. Calibrated sulfur isotope abundance ratios of three IAEA sulfur isotope reference materials and V-CDT with a reassessment of the atomic weight of sulfur. Geochim. Cosmochim. Acta 65, 2433–2437.
Dorendorf, F., Wiechert, U., Wörner, G., 2000. Hydrated sub-arc mantle: a source for the Kluchevskoy volcano, Kamchatka/Russia. Earth Planet. Sci. Lett. 175, 69–86.
Drummond, M.S., Defant, M.J., 1990. A model for trondhjemite-tonalite-dacite genesis and crustal growth via slab melting: Archaean to modern comparisons. J. Geophys. Res. 95, 503–521.
Elliott, T., Plank, T., Zindler, A., White, W., Bourdon, B., 1997. Element transport from slab to volcanic front at the Mariana arc. J. Geophys. Res. 102, 14991–15019.
Esposito, R., Bodnar, R.J., Danyushevsky, L.V., De Vivo, B., Fedele, L., Hunter, J., Lima, A., Shimizu, N., 2011. Volatile evolution of magma associated with the Solchiaro eruption in the Phlegrean Volcanic District (Italy). J. Petrol. 52, 2431–2460.
Fedotov, S.A., Markhinin, Ye.K., 1983. The Great Tolbachik Fissure Eruption. Cambridge Univ. Press, New York.
Fiege, A., Holtz, F., Behrens, H., Mandeville, C.W., Shimizu, N., Crede, L.S., Göttlicher, J., 2015. Experimental investigation of the S and S-isotope distribution between H2O-S ± Cl fluids and basaltic melts during decompression. Chem. Geol. 393–394, 36–54.
Fisher, R.V., Schmincke, H.-U., 1984. Pyroclastic Rocks. Springer-Verlag, Berlin, Heidelberg, New York, Tokyo.
Foley, S.F., Barth, M.G., Jenner, G.A., 2000. Rutile/melt partition coefficients for trace elements and an assessment of the influence of rutile on the trace element characteristics of subduction zone magmas. Geochim. Cosmochim. Acta 64, 933–938.
Francis, P., 1993. Volcanoes: A Planetary Perspective. Clarendon Press, Oxford.
Gill, J.B., 1981. Orogenic Andesites and Plate Tectonics. Springer-Verlag, Berlin-Heidelberg.
Gill, J., Torssander, P., Lapierre, H., Taylor, R., Kaiho, K., Koyama, M., Kusakabe, M., Aitchison, J., Cisowski, S., Dadey, K., Fujioka, K., Klaus, A., Lovell, M., Marsaglia, K., Pezard, P., Taylor, B., Tazaki, K., 1990. Explosive deep-water basalt in the Sumisu Backarc Rift. Science 248, 1214–1217.
Gorshkov, G.S., 1967. Volcanism of the Kurile Island Arc. Nauka, Moscow (in Russian).
Gurenko, A.A., Chaussidon, M., 1997. Boron concentrations and isotopic composition in the Icelandic mantle: evidence from glass inclusions in olivine. Chem. Geol. 135, 21–34.
Gurenko, A.A., Kamenetsky, V.S., 2011. Boron isotopic composition of olivine-hosted melt inclusions from Gorgona komatiites, Colombia: new evidence supporting wet komatiite origin. Earth Planet. Sci. Lett. 312, 201–212.
Gurenko, A.A., Schmincke, H.-U., 2000. S concentrations and its speciation in Miocene basaltic magmas north and south of Gran Canaria (Canary Islands): constraints from glass inclusions in olivine and clinopyroxene. Geochim. Cosmochim. Acta 64, 2321–2337.
Gurenko, A.A., Chaussidon, M., Schmincke, H.-U., 2001. Magma ascent and contamination beneath one intraplate volcano: evidence from S and O isotopes in glass inclusions and their host clinopyroxenes from Miocene basaltic hyaloclastites southwest of Gran Canaria (Canary Islands). Geochim. Cosmochim. Acta 65, 4359–4374.
Gurenko, A.A., Belousov, A.B., Trumbull, R.B., Sobolev, A.V., 2005a. Explosive basaltic volcanism of the Chikurachki Volcano (Kurile arc, Russia): insights on pre-eruptive magmatic conditions and volatile budget revealed from phenocryst-hosted melt inclusions and matrix glasses. J. Volcanol. Geotherm. Res. 147, 203–232.
Gurenko, A.A., Trumbull, R.B., Thomas, R., Lindsay, J.M., 2005b. A melt inclusion record of volatiles, trace elements and Li-B isotope variations in a single magma system from the Plat Pays Volcanic Complex, Dominica, Lesser Antilles. J. Petrol. 46, 2495–2526.
Hartley, M.E., Maclennan, J., Edmonds, M., Thordarson, T., 2014. Reconstructing the deep CO_2 degassing behaviour of large basaltic fissure eruptions. Earth Planet. Sci. Lett. 393, 120–131.
Hasegawa, T., Nakagawa, M., Yoshimoto, M., Ishizuka, Y., Hirose, W., Seki, S.I., Ponomareva, V., Alexander, R., 2011. Tephrostratigraphy and petrological study of Chikurachki and Fuss volcanoes, western Paramushir Island, northern Kurile Islands: Evaluation of Holocene eruptive activity and temporal change of magma system. Quat. Int. 246, 278–297.
Haughton, D.R., Roeder, P.L., Skinner, B.J., 1974. Solubility of sulfur in mafic magmas. Econ. Geol. 69, 541–567.
Hawkesworth, C.J., Gallagher, K., Hergt, J.M., McDermott, F., 1993. Mantle and slab contributions in arc magmas. Annu. Rev. Earth Planet. Sci. 21, 175–204.
Hickey, R.L., Frey, F.A., 1982. Geochemical characteristics of boninite series volcanics: implications for their source. Geochim. Cosmochim. Acta 46, 2099–2115.
Hickey, R., Frey, F.A., Gerlach, D.C., Lopez-Escobar, L., 1986. Multiple sources for basaltic arc rocks from the southern volcanic zone of the Andes (34°–41°S): trace element and isotopic evidence for contributions from subducted oceanic crust, mantle and continental crust. J. Geophys. Res. 91, 5963–5983.
Hochstaedter, A.G., Kepezhinskas, P., Defant, M., 1996. Insights into volcanic arc mantle wedge from magnesian lavas from the Kamchatka arc. J. Geophys. Res. 101, 697–712.
Hochstaedter, A., Gill, J., Peters, R., Broughton, P., Holden, P., Taylor, B., 2001. Across-arc geochemical trends in the Izu-Bonin arc: contributions from the subducting slab. Geochem. Geophys. Geosyst. 2 (2000GC000105).
Hofmann, A.W., 1988. Chemical differentiation of the Earth: the relationship between mantle, continental crust and oceanic crust. Earth Planet. Sci. Lett. 90, 297–314.
Holloway, J.R., Blank, J.G., 1994. Application of experimental results to C-O-H species in natural melts. In: Carroll, M.R., Holloway, J.R. (Eds.), Volatiles in Magmas. Reviews in Mineralogy 30. Mineralogical Society of America, Washington, D.C., pp. 187–230.
Houghton, B.F., Gonnermann, H.M., 2008. Basaltic explosive volcanism: constraints from deposits and models. Chem. Erde 68, 117–140.
Houghton, B.F., Wilson, C.J.N., Del Carlo, P., Coltelli, M., Sable, J.E., Carey, R., 2004. The influence of conduit processes on changes in style of basaltic Plinian eruptions: Tarawera 1886 and Etna 122 BC. J. Volcanol. Geotherm. Res. 137, 1–14.
Ikeda, Y., 1998. Geochemistry of Miocene back-arc basin basalts from northeast Hokkaido, Japan. J. Geol. Soc. Jpn. 104, 99–106.
Ikeda, Y., Stern, R.J., Kagami, H., Sun, C.-H., 2000. Pb, Nd, and Sr isotopic constraints on the origin of Miocene basaltic rocks from northeast Hokkaido, Japan: implications for opening of the Kurile back-arc basin. Island Arc 9, 161–172.
Ishikawa, T., Nakamura, E., 1992. Boron isotope geochemistry of the oceanic crust from DSDP/ODP hole 504B. Geochim. Cosmochim. Acta 56, 1633–1639.
Ishikawa, T., Tera, F., 1997. Source, composition and distribution of the fluid in the Kurile mantle wedge: constraints from across-arc variations of B/Nb and B isotopes. Earth Planet. Sci. Lett. 152, 123–138.
Ishikawa, T., Tera, F., Nakazawa, T., 2001. Boron isotope and trace element systematics of the three volcanic zones in the Kamchatka arc. Geochim. Cosmochim. Acta 65, 4523–4537.
Jambon, A., 1994. Earth degassing and large-scale geochemical cycling of volatile elements. In: Carroll, M.R., Holloway, J.R. (Eds.), Volatiles in Magmas. Reviews in Mineralogy 30. Mineralogical Society of America, Washington, D.C., pp. 479–517.
Jambon, A., Déruelle, B., Dreibus, G., Pineau, F., 1995. Chlorine and bromine abundance in MORB: the contrasting behaviour of the Mid-Atlantic Ridge and East Pacific Rise and implications for chlorine geodynamic cycle. Chem. Geol. 126, 101–117.
Johnson, M.C., Plank, T., 1999. Dehydratation and melting experiments constrain the fate of subducted sediments. Geochem. Geophys. Geosyst. 1 (1999GC000014).
Jugo, P.J., Luth, R.W., Richards, J.P., 2005a. Experimental data on the speciation of sulfur as a function of oxygen fugacity in basaltic melts. Geochim. Cosmochim. Acta 69, 497–503.
Jugo, P.J., Luth, R.W., Richards, J.P., 2005b. An experimental study of the sulfur content in basaltic melts saturated with immiscible sulfide or sulfate Liquids at 1300 °C and 1.0 GPa. J. Petrol. 46, 783–798.
Jugo, P.J., Wilke, M., Botcharnikov, R.E., 2010. Sulfur K-edge XANES analysis of natural and synthetic basaltic glasses: implications for S speciation and S content as function of oxygen fugacity. Geochim. Cosmochim. Acta 74, 5926–5938.
Kamenetsky, V.S., Crawford, A.J., Eggins, S., Mühe, R., 1997. Phenocryst and melt inclusion chemistry of near-axis seamounts, Valu Fa Ridge, Lau basin: insight into mantle wedge melting and the addition of subduction components. Earth Planet. Sci. Lett. 151, 205–223.
Katsura, T., Nagashima, S., 1974. Solubility of sulfur in some magmas at 1 atmosphere. Geochim. Cosmochim. Acta 38, 517–531.
Kay, R.W., 1978. Aleutian magnesian andesites: melts from subducted Pacific ocean crust. J. Volcanol. Geotherm. Res. 4, 117–132.
Kendrick, M.A., Arculus, R., Burnard, P., Honda, M., 2013. Quantifying brine assimilation by submarine magmas: examples from the Galápagos Spreading Centre and Lau Basin. Geochim. Cosmochim. Acta 123, 150–165.
Kent, A.J.R., Norman, M.D., Hutcheon, I.D., Stolper, E.M., 1999. Assimilation of seawater-derived components in an oceanic volcano: evidence from matrix glasses and glass inclusions from Loihi seamount, Hawaii. Chem. Geol. 156, 299–319.
Kepezhinskas, P., McDermott, F., Defant, M.J., Hochstaedter, A., Drummond, M.S., Hawkesworth, C., Koloskov, A., Maury, R.C., Bellon, H., 1997. Trace element and Sr-Nd-Pb isotopic constraints on a three-component model of Kamchatka Arc petrogenesis. Geochim. Cosmochim. Acta 61, 577–600.
Khubunaya, S.A., Sobolev, A.V., 1998. Primary melts of calc-alkaline magnesian basalts from the Klyuchevskoi volcano, Kamchatka. Dokl. Akad. Nauk 360, 100–102.
Konrad-Schmolke, M., Halama, R., Manea, V.C., 2016. Slab mantle dehydrates beneath Kamchatka – Yet recycles water into the deep mantle. Geochem. Geophys. Geosyst. 17, 2987–3007.
Kress, V., 1997. Magma mixing as a source for Pinatubo sulphur. Nature 389, 591–593.
Langmuir, C.H., Vocke, R.D., Hanson, G.N., Hart, S.R., 1978. A general mixing equation with applications to Icelandic basalts. Earth Planet. Sci. Lett. 37, 380–392.
Lassiter, J.C., Hauri, E.H., Nikogosian, I.K., Barsczus, H.G., 2002. Chlorine-potassium variations in melt inclusions from Raivavae and Rapa, Austral Islands: constraints on chlorine recycling in the mantle and evidence for brine-induced melting of oceanic crust. Earth Planet. Sci. Lett. 202, 525–540.
Le Voyer, M., Rose-Koga, E.F., Laubier, M., Schiano, P., 2008. Petrogenesis of arc lavas from the Rucu Pichincha and Pan de Azucar volcanoes (Ecuadorian arc): major, trace element, and boron isotope evidences from olivine-hosted melt inclusions. Geochem. Geophys. Geosyst. 9. http://dx.doi.org/10.11029/12008GC002173.
Le Voyer, M., Cottrell, E., Kelley, K.A., Brounce, M., Hauri, E.H., 2015. The effect of primary versus secondary processes on the volatile content of MORB glasses: an example from the equatorial Mid-Atlantic ridge (5°N–3°S). J. Geophys. Res. 120 (2014JB011160).
Leeman, W.P., Sisson, V.B., 1996. Geochemistry of boron and its implications for crustal and mantle processes. In: Grew, E.S., Anovitz, L.M. (Eds.), Boron: Mineralogy, Petrology and Geochemistry. 33. Mineralogical Society of America, Washington, D.C., pp. 645–707.

Leeman, W.P., Tonarini, S., Chan, L.H., Borg, L.E., 2004. Boron and lithium isotopic variations in a hot subduction zone—the southern Washington cascades. Chem. Geol. 212, 101–124.
Luhr, J.F., 1990. Experimental phase relations of water and sulfur saturated arc magmas and the 1982 eruptions of El Chichón volcano. J. Petrol. 31, 1071–1114.
Luhr, J.F., Carmichael, I.S.E., Varekamp, J.C., 1984. The 1982 eruptions of El Chichón volcano, Chiapas, Mexico: mineralogy and petrology of the anhydrite-bearing pumices. J. Volcanol. Geotherm. Res. 23, 69–108.
Macpherson, C.G., Mattey, D.P., 1998. Oxygen isotope variations in Lau Basin lavas. Chem. Geol. 144, 177–194.
Mandeville, C.W., Webster, J.D., Tappen, C., Taylor, B.E., Timbal, A., Sasaki, A., Hauri, E., Bacon, C.R., 2009. Stable isotope and petrologic evidence for open-system degassing during the climactic and pre-climactic eruptions of Mt. Mazama, Crater Lake, Oregon. Geochim. Cosmochim. Acta 73, 2978–3012.
Marini, L., Moretti, R., Accornero, M., 2011. Sulfur isotopes in magmatic-hydrothermal systems, melts, and magmas. Rev. Mineral. Geochem. 73, 423–492.
Mathez, E.A., 1976. Sulfur solubility and magmatic sulfides in submarine basalt glasses. J. Geophys. Res. 81, 4269–4276.
Matjuschkin, V., Blundy, J.D., Brooker, R.A., 2016. The effect of pressure on sulphur speciation in mid- to deep-crustal arc magmas and implications for the formation of porphyry copper deposits. Contrib. Mineral. Petrol. 171, 66.
Mavrogenes, J., Blundy, J., 2017. Crustal sequestration of magmatic sulfur dioxide. Geology 45, 211–214.
Mavrogenes, J.A., O'Neill, H.S.C., 1999. The relative effects of pressure, temperature and oxygen fugacity on the solubility of sulfide in mafic magmas. Geochim. Cosmochim. Acta 63, 1173–1180.
McCulloch, M.T., Gamble, J.A., 1991. Geochemical and geodynamical constraints on subduction zone magmatism. Earth Planet. Sci. Lett. 102, 358–374.
Metrich, N., Clocchiatti, R., 1996. Sulfur abundance and its speciation in oxidized alkaline melts. Geochim. Cosmochim. Acta 60, 4151–4160.
Métrich, N., Schiano, P., Clocchiatti, R., Maury, R.C., 1999. Transfer of sulfur in subduction settings: an example from Batan Island (Luzon volcanic arc, Philippines). Earth Planet. Sci. Lett. 167, 1–14.
Michael, P.J., Cornell, W.C., 1998. Influence of spreading rate and magma supply on crystallisation and assimilation beneath mid-ocean ridges: evidence from chlorine and major element chemistry of mid-ocean ridge basalts. J. Geophys. Res. 103, 18325–18356.
Michael, P., Schilling, J.-G., 1989. Chlorine in mid-ocean ridge magmas: evidence for assimilation of seawater-influenced components. Geochim. Cosmochim. Acta 53, 3131–3143.
Mironov, N., Portnyagin, M., Botcharnikov, R., Gurenko, A., Hoernle, K., Holtz, F., 2015. Quantification of the CO_2 budget and H_2O–CO_2 systematics in subduction-zone magmas through the experimental hydration of melt inclusions in olivine at high H_2O pressure. Earth Planet. Sci. Lett. 425, 1–11.
Miyoshi, T., Sakai, H., Chiba, H., 1984. Experimental study of sulfur isotope fractionation factors between sulfate and sulfide in high temperature melts. Geochem. J. 18, 75–84.
Moore, L.R., Gazel, E., Tuohy, R., Lloyd, A.S., Esposito, R., Steele-MacInnis, M., Hauri, E.H., Wallace, P.J., Plank, T., Bodnar, R.J., 2015. Bubbles matter: an assessment of the contribution of vapor bubbles to melt inclusion volatile budgets. Am. Mineral. 100, 806–823.
Nagashima, S., Katsura, T., 1973. The solubility of sulfur in Na2O-SiO2 melts under various oxygen partial pressures at 1200, 1250 and 1300° C. Bull. Chem. Soc. Japan 46, 3099–3103.
Newman, S., Lowenstern, J.B., 2002. VolatileCalc: a silicate melt-H_2O-CO_2 solution model written in Visual Basic for Excel. Comput. Geosci. 28, 597–604.
Ovsyannikov, A.A., Muravyev, Y.D., 1992. Eruptions of the Chikurachki volcano. Volcanol. Seismol. 5-6, 3–21 (in Russian).
Peacock, S.M., Hervig, R.L., 1999. Boron isotopic composition of subduction-zone metamorphic rocks. Chem. Geol. 160, 281–290.
Pearce, J.A., 1983. Role of the sub-continental lithosphere in magma genesis at active continental margins. In: Hawkesworth, C.J., Norry, M.J. (Eds.), Continental Basalts and Mantle Xenoliths. Shiva Publishing, Nantwich, UK, pp. 230–249.
Pearce, J.A., Peate, D.W., 1995. Tectonic implications of the composition of volcanic arc magmas. Annu. Rev. Earth Planet. Sci. 24, 251–285.
Plank, T., Langmuir, C.H., 1998. The chemical composition of subducting sediment and its consequences for the crust and mantle. Chem. Geol. 145, 325–394.
Portnyagin, M., Hoernle, K., Plechov, P., Mironov, N., Khubunaya, S., 2007. Constraints on mantle melting and composition and nature of slab components in volcanic arcs from volatiles (H_2O, S, Cl, F) and trace elements in melt inclusions from the Kamchatka Arc. Earth Planet. Sci. Lett. 255, 53–69.
Portnyagin, M., Duggen, S., Hauff, F., Mironov, N., Bindeman, I., Thirlwall, M., Hoernle, K., 2015. Geochemistry of the Late Holocene rocks from the Tolbachik volcanic field, Kamchatka: quantitative modelling of subduction-related open magmatic systems. J. Volcanol. Geotherm. Res. 307, 133–155.
Richet, P., Bottinga, Y., Javoy, M., 1977. A review of hydrogen, carbon, nitrogen, oxygen, sulfur and chlorine stable isotope fractionation among gaseous molecules. Annu. Rev. Earth Planet. Sci. 5, 65–110.
Robin, C., Eissen, J.P., Monzier, M., 1993. Giant tuff cone and 12-km-wide associated caldera at Ambrym volcano (Vanuatu, New Hebrides Arc). J. Volcanol. Geotherm. Res. 55, 225–238.
Rogers, G., Saunders, A.D., Terrell, D.J., Verma, S.P., Marriner, G.F., 1985. Geochemistry of Holocene volcanic rocks associated with ridge subduction in Baja, California, Mexico. Nature 315, 389–392.
Roggensack, K., Hervig, R.L., McKnight, S.B., Williams, S.N., 1997. Explosive basaltic volcanism from Cerro Negro volcano: influence of volatiles on eruptive style. Science 277, 1639–1642.
Rose, E.F., Shimizu, N., Layne, G.D., Grove, T.L., 2001. Melt production beneath Mt. Shasta from boron data in primitive melt inclusions. Science 293, 281–283.
Rosner, M., Erzinger, J., Franz, G., Trumbull, R.B., 2003. Slab-derived boron isotope signatures in arc volcanic rocks from the Central Andes and evidence for boron isotope fractionation during progressive slab dehydration. Geochem. Geophys. Geosyst. 4. http://dx.doi.org/10.1029/2002GC000438.
le Roux, P.J., Shirey, S.B., Hauri, E.H., Perfit, M.R., Bender, J.F., 2006. The effects of variable sources, processes and contaminants on the composition of northern EPR MORB (8–10°N and 12–14°N): Evidence from volatiles (H_2O, CO_2, S) and halogens (F, Cl). Earth Planet. Sci. Lett. 251, 209–231.
Ruth, D.C.S., Cottrell, E., Cortés, J.A., Kelley, K.A., Calder, E.S., 2016. From passive degassing to violent strombolian eruption: the case of the 2008 eruption of Llaima volcano, Chile. J. Petrol. 57, 1833–1864.
Ryan, J.G., Langmuir, C.H., 1993. The systematics of boron abundances in young volcanic rocks. Geochim. Cosmochim. Acta 57, 1489–1498.
Ryan, J.G., Morris, J., Tera, F., Leeman, W.P., Tsvetkov, A., 1995. Cross-arc geochemical variations in the Kurile Arc as a function of slab depth. Science 270, 625–627.
Saal, A.E., Hauri, E.H., Langmuir, C.H., Perfit, M.R., 2002. Vapour undersaturation in primitive mid-ocean-ridge basalt and the volatile content of Earth's upper mantle. Nature 419, 451–455.
Sable, J.E., Houghton, B.F., Del Carlo, P., Coltelli, M., 2006. Changing conditions of magma ascent and fragmentation during the Etna 122 BC basaltic Plinian eruption: Evidence from clast microtextures. J. Volcanol. Geotherm. Res. 158, 333–354.
Sakai, H., Casadevall, T.J., Moore, J.G., 1982. Chemistry and isotopic ratios of sulfur in basalts and volcanic gases at Kilauea volcano, Hawaii. Geochim. Cosmochim. Acta 46, 729–738.
Sakai, H., Des Marais, D.J., Ueda, A., Moore, J.G., 1984. Concentrations and isotope ratios of carbon, nitrogen and sulfur in ocean floor basalt. Geochim. Cosmochim. Acta 48, 2433–2441.
Salters, V.J.M., Stracke, A., 2004. Composition of the depleted mantle. Geochem. Geophys. Geosyst. 5. http://dx.doi.org/10.1029/2003GC000597.
Savov, I.P., Ryan, J.G., D'Antonio, M., Kelley, K., Mattie, P., 2005. Geochemistry of serpentinized peridotites from the Mariana Forearc-Conical Seamount, ODP Leg 125: implications for the elemental recycling at subduction zones. Geochem. Geophys. Geosyst. 6, Q04J15. http://dx.doi.org/10.1029/2004GC000777.
Savov, I.P., Ryan, J.G., D'Antonio, M., Fryer, P., 2007. Shallow slab fluid release across and along the Mariana arc-basin system: insights from geochemistry of serpentinized peridotites from the Mariana Forearc. J. Geophys. Res. 112. http://dx.doi.org/10.1029/2006JB004749.
Scambelluri, M., Tonarini, S., 2012. Boron isotope evidence for shallow fluid transfer across subduction zones by serpentinized mantle. Geology 40, 907–910.
Selvaraja, V., Fiorentini, M.L., LaFlamme, C.K., Wing, B.A., Bui, T.-H., 2017. Anomalous sulfur isotopes trace volatile pathways in magmatic arcs. Geology 45, 419–422.
Shaw, D.M., 1970. Trace element fractionation during anatexis. Geochim. Cosmochim. Acta 34, 237–243.
Shimizu, K., Shimizu, N., Komiya, T., Suzuki, K., Maruyama, S., Tatsumi, Y., 2009. CO_2-rich komatiitic melt inclusions in Cr-spinels within beach sand from Gorgona Island, Colombia. Earth Planet. Sci. Lett. 288, 33–43.
Shinohara, H., 2008. Excess degassing from volcanoes and its role on eruptive and intrusive activity. Rev. Geophys. 46, RG4005. http://dx.doi.org/10.1029/2007RG000244.
Simons, K., Dixon, J., Schilling, J.-G., Kingsley, R., Poreda, R., 2002. Volatiles in basaltic glasses from the Easter-Salas y Gomez seamount chain and Easter microplate: implications for geochemical cycling of volatile elements. Geochem. Geophys. Geosyst. 3. http://dx.doi.org/10.1029/2001GC000173.
Smith, H.J., Leeman, W.P., Davidson, J., Spivack, A.J., 1997. The B isotopic composition of arc lavas from Martinique, Lesser Antilles. Earth Planet. Sci. Lett. 146, 303–314.
Smythe, D.J., Wood, B.J., Kiseeva, E.S., 2017. The S content of silicate melts at sulfide saturation: new experiments and a model incorporating the effects of sulfide composition. Am. Mineral. 102, 795–803.
Soto, G.J., Alvarado, G.E., 2006. Eruptive history of Arenal Volcano, Costa Rica, 7 ka to present. J. Volcanol. Geotherm. Res. 157, 254–269.
Spivack, A.J., Edmond, J.M., 1986. Determination of boron isotope ratios by thermal ionization mass spectrometry of the dicesium metaborate cation. Anal. Chem. 58, 31–35.
Stalder, R., Foley, S.F., Brey, G.P., Horn, I., 1998. Mineral-aqueous fluid partitioning of trace elements at 900–1200 °C and 3.0–5.7 GPa: new experimental data for garnet, clinopyroxene, and rutile, and implications for mantle metasomatism. Geochim. Cosmochim. Acta 62, 1781–1801.
Staudigel, H., Plank, T., White, B., Schmincke, H.-U., 1996. Geochemical fluxes during seafloor alteration of the basaltic upper oceanic crust: DSDP Sites 417 and 418. In: Bebout, G.E., Scholl, D.W., Kirby, S.H., Platt, J.P. (Eds.), Subduction: Top to Bottom. Geophysical Monography 96. American Geophysical Union, pp. 19–38.
Steele-Macinnis, M., Esposito, R., Bodnar, R.J., 2011. Thermodynamic model for the effect of post-entrapment crystallization on the H_2O–CO_2 systematics of vapor-saturated, silicate melt inclusions. J. Petrol. 52, 2461–2482.
Stern, C.R., Kilian, R., 1996. Role of the subducted slab, mantle wedge and continental crust in the generation of adakites from the Andean Austral Volcanic Zone. Contrib. Mineral. Petrol. 123, 263–281.
Stern, C.R., Futa, K., Muehlenbachs, K., 1984. Isotope and trace element data for orogenic andesites from the Austral Andes. In: Harmon, R.S., Barreiro, B.A. (Eds.), Andean Magmatism: Chemical and Isotopic Constraints. Shiva Publishing, Cheshire, UK, pp. 31–46.
Straub, S.M., Layne, G.D., 2002. The systematics of boron isotopes in Izu arc front volcanic rocks. Earth Planet. Sci. Lett. 198, 25–39.

Straub, S.M., Layne, G.D., 2003. The systematics of chlorine, fluorine, and water in Izu arc front volcanic rocks: implications for volatile recycling in subduction zones. Geochim. Cosmochim. Acta 67, 4179–4203.
Symonds, R.B., Rose, W.I., Bluth, G.J.S., Gerlach, T.M., 1994. Volcanic-gas studies: methods, results, and applications. In: Carroll, M.R., Holloway, J.R. (Eds.), Volatiles in Magmas. Reviews in Mineralogy 30. Mineralogical Society of America, Washington, D.C., pp. 1–66.
Szramek, L., Gardner, J.E., Larsen, J., 2006. Degassing and microlite crystallization of basaltic andesite magma erupting at Arenal Volcano, Costa Rica. J. Volcanol. Geotherm. Res. 157, 182–201.
Szramek, L., Gardner, J.E., Hort, M., 2010. Cooling-induced crystallization of microlite crystals in two basaltic pumice clasts. Amer. Mineral. 95, 503–509.
Takagi, T., Orihashi, Y., Naito, K., Watanabe, Y., 1999. Petrology of a mantle-derived rhyolite, Hokkaido, Japan. Chem. Geol. 160, 425–445.
Tatsumi, Y., Hamilton, D.L., Nesbitt, R.W., 1986. Chemical characteristics of fluid phase released from a subducted lithosphere and origin of arc magmas: evidence from high-pressure experiments and natural rocks. J. Volcanol. Geotherm. Res. 29, 293–309.
Tatsumi, Y., Furukawa, Y., Kogiso, T., Yamada, Y., Yokoyama, T., Fedotov, S.A., 1994. A third volcanic chain in Kamchatka: Thermal anomaly at transform/convergence plate boundary. Geophys. Res. Lett. 21, 537–540.
Taylor, B.E., 1986. Magmatic Volatiles: Isotopic Variation of C, H, and S. In: Valley, J.W., Taylor Jr.H.P., O'Neil, J.R. (Eds.), Stable Isotopes in High Temperature Geological Processes. Reviews in Mineralogy Vol. 16. Mineralogical Society of America, Washington, D.C., pp. 185–225.
Thirlwall, M.F., Graham, A.M., Arculus, R.J., Harmon, R.S., Macpherson, C.G., 1996. Resolution of the effects of crustal assimilation, sediment subduction, and fluid transport in island arc magmas: Pb-Sr-Nd-O isotope geochemistry of Grenada, Lesser Antilles. Geochim. Cosmochim. Acta 60, 4785–4810.
Tonarini, S., Leeman, W.P., Leat, P.T., 2011. Subduction erosion of forearc mantle wedge implicated in the genesis of the South Sandwich Island (SSI) arc: evidence from boron isotope systematics. Earth Planet. Sci. Lett. 301, 275–284.
Turner, S., Hawkesworth, C., Rogers, N., Bartlett, J., Worthington, T., Hergt, J., Pearce, J.A., Smith, I., 1997. ^{238}U-^{230}Th disequilibria, magma petrogenesis, and flux rates beneath the depleted Tonga-Kermadec island arc. Geochim. Cosmochim. Acta 61, 4855–4884.
Varekamp, J.C., Luhr, J.F., Prestegaard, K.L., 1984. The 1982 eruptions of El Chichón volcano (Chiapas, Mexico): character of the eruptions, ash-fall deposits, and gas phase. J. Volcanol. Geotherm. Res. 23, 39–68.
Vroon, P.Z., Lowry, D., van Bergen, M.J., Boyce, A.J., Mattey, D.P., 2001. Oxygen isotope systematics of the Banda Arc: low $\delta^{18}O$ despite involvement of subducted continental material in magma genesis. Geochim. Cosmochim. Acta 65, 589–609.
Walker, G.P.L., 1973. Explosive volcanic eruptions – a new classification scheme. Geol. Rundsch. 62, 431–446.
Walker, G.P.L., 1980. The Taupo pumice: product of the most powerful known (ultra-plinian) eruption? J. Volcanol. Geotherm. Res. 8, 69–94.
Walker, G.P.L., Self, S., Wilson, L., 1984. Tarawera 1886, New Zealand — a basaltic plinian fissure eruption. J. Volcanol. Geotherm. Res. 21, 61–78.
Wallace, P.J., Anderson, A.T.J., 1998. Effects of eruption and lava drainback on the H_2O contents of basaltic magmas at Kilauea Volcano. Bull. Volcanol. 59, 327–344.
Wallace, P., Carmichael, I.S.E., 1992. Sulfur in basaltic magmas. Geochim. Cosmochim. Acta 56, 1863–1874.
Wallace, P.J., Carmichael, I.S.E., 1994. S speciation in submarine basaltic glasses as determined by measurements of SK_α X-ray wavelength shifts. Am. Mineral. 79, 161–167.
Wallace, P.J., Kamenetsky, V.S., Cervantes, P., 2015. Melt inclusion CO_2 contents, pressures of olivine crystallization, and the problem of shrinkage bubbles. Am. Mineral. 100, 787–794.
Walowski, K.J., Wallace, P.J., Clynne, M.A., Rasmussen, D.J., Weis, D., 2016. Slab melting and magma formation beneath the southern Cascade arc. Earth Planet. Sci. Lett. 446, 100–112.
Williams, S.N., 1983. Plinian airfall deposits of basaltic composition. Geology 11, 211–214.
Wilson, L., Walker, G.P.L., 1987. Explosive volcanic eruptions – VI. Ejecta dispersal in plinian eruptions: the control of eruption conditions and atmospheric properties. Geophys. J. R. Astron. Soc. 89, 657–679.
Woodhead, J., Eggins, S., Gamble, J., 1993. High field strength and transition element systematics in island arc and back-arc basin basalts: evidence for multi-phase melt extraction and a depleted mantle wedge. Earth Planet. Sci. Lett. 114, 491–504.
Wunder, B., Meixner, A., Romer, R.L., Wirth, R., Heinrich, W., 2005. The geochemical cycle of boron: constraints from boron isotope partitioning experiments between mica and fluid. Lithos 84, 206–216.
Yogodzinski, G.M., Lees, J.M., Churikova, T.G., Dorendorf, F., Wörner, G., Volynets, O.N., 2001. Geochemical evidence for the melting of subducting oceanic lithosphere at plate edges. Nature 409, 500–504.